F
N
P

JOURNAL OF FOOD PROCESS ENGINEERING

D.R. HELDMAN
and
R.P. SINGH
COEDITORS

JOURNAL OF FOOD PROCESS ENGINEERING

JOURNAL OF FOOD PROCESS ENGINEERING

JOURNAL OF FOOD PROCESS ENGINEERING

Printed in the United States of America

CONTENTS

ORIFICE DISCHARGE COEFFICIENTS
FOR POWER-LAW FLUIDS

WALTER F. SALAS-VALERIO

Universidad Nacional Agraria, La Molinia, Lima, Peru

and

JAMES F. STEFFE

Department of Agricultural Engineering
Department of Food Science and Human Nutrition
Michigan State University
East Lansing, MI 48824-1323

ABSTRACT

Orifice discharge coefficients for non-Newtonian (power-law) fluids (5, 7.5 and 10% corn starch solutions) were measured using a closed end pipe with different orifice diameters. Results indicate that orifice discharge coefficients, found to be in the range of 0 – 0.7, are a function of the orifice diameter, fluid velocity in the orifice and the fluid rheological properties (consistency coefficient and flow behavior index). They increase with the fluid velocity, tend to be constant at high velocities and decrease when the consistency coefficient of the solution is increasing. Orifice discharge coefficients are presented as a function of the generalized Reynolds number.

INTRODUCTION

Pumping systems are used in many food processing operations and, in special cases, they pump fluid into perforated pipes causing the material to move through small orifices. Applications may include distribution of frosting on to a continuous conveyer holding breakfast rolls or distribution of fluid into a plate heat exchanger. Many fluids encountered in the food industry are non-Newtonian and engineers working with these materials cannot predict the orifice flow rates because of the lack of data for orifice discharge coefficients. The *objective* of this study was to determine orifice discharge coefficients for non-Newtonian fluids and to analyze their behavior with respect to orifice diameter, fluid velocity and fluid properties.

[1]Direct correspondence to Dr. J.F. Steffe, Dept. of Agric. Engr.

LITERATURE REVIEW

In contrast to the concentration of effort on the problem of Newtonian fluid flow in orifices (orifice and Venturi meters), the problem for non-Newtonian fluids has been almost ignored. Consult Perry and Green (1984) for general references related to Newtonian fluids.

Vennard and Street (1975) state that orifice discharge coefficients (C) for Newtonian fluids are found over a wide range of Reynolds numbers, where Reynolds numbers are defined on the basis of flow rate in the orifice and orifice diameter. The orifice discharge coefficients are in the range of 0.6–0.9 and are affected by the fluid viscosity and the size of the vena contracta in the orifice. In the case where the orifice coefficient is determined for the static pressure (large reservoir with an orifice on the wall) and discharge to the atmosphere, the discharge coefficient depends upon the shape of the orifice as well as fluid viscosity and the size of the vena contracta (Vennard and Street 1975). DeCarlo (1984) notes that the orifice discharge coefficient accounts for the energy lost in the orifice due to friction and the actual pressure drop is larger than the theoretical value calculated using the ideal fluid concept.
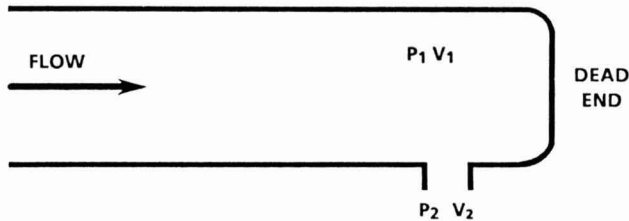
FIGURE 1.

FIG. 1. PIPE WITH A SINGLE ORIFICE AND A DEAD END

THEORETICAL CONSIDERATIONS

Consider an incompressible, time-independent fluid flowing in a single orifice pipe with dead end (Fig. 1). Applying the mechanical energy balance between point 1 (in the main pipe, subscript 1) and point 2 (the outlet of the orifice, subscript 2) yields:

$$p_1/\rho + v_1^2/\alpha_1 + z_1 g = p_2/\rho + v_2^2/\alpha_2 + z_2 g + k_0 v_2^2/2 \qquad (1)$$

Rearranging terms, assuming that the distance z_1 is equal to z_2 (because the pressure drop due to change in potential energy is negligible compared to the other factors) and p_2 is zero (fluid exits to atmospheric pressure) gives

$$v_2^2 = \frac{p_1/\rho + v_1^2/\alpha_1}{k_0/2 + 1/\alpha_2} \qquad (2)$$

or

$$q_2 = \rho A C [p_1/\rho + v_1^2/\alpha_1]^{1/2} \qquad (3)$$

where

$$C = [k_0/2 + 1/\alpha_2]^{-1/2} \qquad (4)$$

The discharge coefficient may be a function of the fluid properties, velocity, orifice diameter and so on; hence it is necessary to experimentally determine exact values. The kinetic energy correction factor is a function of rheological properties and may be calculated using the equation developed by Osorio and Steffe (1984).

MATERIALS AND METHODS

Experimental Materials

A modified waxy maize food starch (National 150: National Starch and Chemical Co., Bridgewater, New Jersey) was used in the experiments. The starch was obtained as white powder containing 11% moisture (wet basis). Aqueous solutions were prepared by first weighing the correct amount of water into a mixing tank, starting the mixer, and slowly pouring in starch until the required amount was added. The mixture was heated at 68 °C until starch gelatinization was obtained, and the mixture had the appropriate thickness. After agitation, the mixer was shut off and the solution was allowed to cool (overnight) to room temperature. Tap water (pH = 7.5) was used to prepare aqueous solutions of 5, 7.5 and 10% (wet basis) starch. The total solid contents (used to verify starch concentration) were determined using an oven drying test: 103 °C for 24 h. Fluid density was measured with a graduate cylinder and an analytical balance. A Haake RV-12 concentric cylinder viscometer was used to measure the rheological behavior of the starch solution. Bob speed was controlled with a Haake PG-12 connected to the drive head of the viscometer and data were collected using a Hewlett-Packard data acquisition system. All samples were obtained directly (after discharge) from the orifice. Once the product was in the Haake sample cup, temperature was controlled with a jacketed temperature

vessel and water bath system (Haake FC-3). All testing was performed at approximately 22 °C over a speed range of 10–150 rpm, resulting in a shear rate range of 20–250 s^{-1}, depending on the product. Twenty data points were collected for each test and the method outlined by Krieger (1968) was used to calculate the shear rate.

Experimental Orifice System and Data Collection

Trials were carried out in an experimental manifold system (Fig. 2). The unit included a Waukesha, Model 10, rotary pump with variable speed drive. Threaded PVC, schedule #40, with an 0.0409m inside diameter and a length of 0.5m was used as a main pipe. The orifice was located at one end and a manometer was installed diametrically opposite the orifice to measure the pressure at that point. Three orifice diameters (0.00318, 0.00476 and 0.0784m) and various flow rates were used in the experiments.
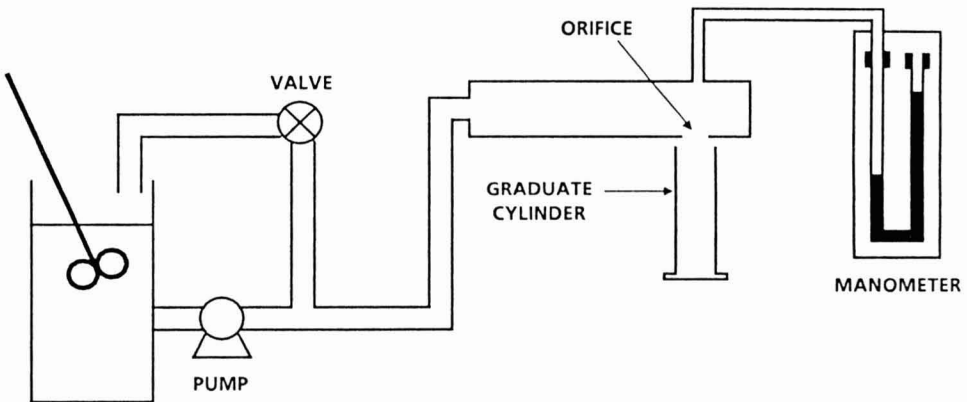
FIGURE 2.

FIG. 2. EXPERIMENTAL EQUIPMENT USED TO COLLECT ORIFICE FLOW RATE
AND PRESSURE DROP DATA

To study the effect of orifice diameter and flow rate on the orifice discharge coefficient, a series of steps were followed. A starch solution was selected and pumped through the experimental system (Fig. 2) with a fixed orifice diameter. Flow rate through the orifice was varied by adjusting the variable speed rotary pump and bypass system. Volumetric flow rate was measured by collecting (in a graduate cylinder) and weighing samples after a fixed period of time. The pressure drop was observed by reading the manometer. Samples were taken for

rheological measurements and the determination of fluid density. The above steps were repeated for different starch solutions, orifice diameters and orifice flow rates.

Calculation of the Orifice Discharge Coefficient

The orifice discharge coefficient was calculated from Eq. (3), using the necessary data: mass flow rate, pressure, density, orifice diameter and kinetic energy coefficient. Discharge coefficients were plotted, versus mass flow rate, and a mathematical expression was obtained giving the orifice discharge coefficient as a function of mass flow rate when the orifice diameter and the rheological properties of the fluid were kept constant. In this way, three mathematical functions for each orifice diameter and three mathematical functions for each fluid, for a total of nine equations, were obtained.

Fluid Properties

All fluids were found to follow the power-law model (Whorlow 1980) over the shear rate range tested (20–250 s^{-1}). Properties (at 22 °C) of the gelatinized corn starch solutions used in the experiment are summarized in Table 1. The total solids content, density, and consistency coefficient decrease as the starch concentration decreases, but the flow behavior index increases. Rheological data indicated no time-dependent behavior or yield stress in the material.

TABLE 1.
PROPERTIES (AT 22 °C) OF GELATINIZED CORN STARCH SOLUTIONS

Solids Content % wet basis	Density kg/m³	Consistency Coefficient Pa s^a	Flow Behavior Index dimensionless
5.0	1010	0.105	0.80
7.5	1020	1.300	0.77
10.0	1034	4.500	0.68

Orifice Discharge Coefficient

Calculating C values with and without including the kinetic energy term (Eq. 3) created differences of less than 3%. Therefore Eq. (3) was simplified, by deleting the kinetic energy term, leaving the following governing expression:

$$q_2 = A\rho C (2p_1/\rho)^{1/2} \tag{5}$$

Three separate sets of orifice discharge coefficient data for each starch solution were generated using the simplified expression (Eq. 5). Figure 3, 4 and 5 show the results indicating that C values are a function of the orifice diameter, fluid velocity and rheological properties. Using a 0.00318 m orifice diameter, 0.105 Pa s^n consistency coefficient and a 0.8 flow behavior index (Fig. 3), the C values start from zero and increase with the fluid velocity. However, they tend to be a constant value in the range of C values from 0.45 to 0.50. Investigations indicate that experimental data (Fig. 3) for each orifice diameter follow the same pattern. Also, a comparison among Fig. 3, 4 and 5 shows that the orifice discharge coefficient tends to be a constant at high fluid velocities but decreases when the solid content of the solution is increasing. Each set of orifice discharge coefficient data was analyzed as a function of the fluid velocity in the orifice. The distribution of the data (Fig. 3, 4, and 5) follows an exponential mathematical model:

$$C = B_1(1 - \exp(-B_2 v)) \qquad\qquad (6)$$
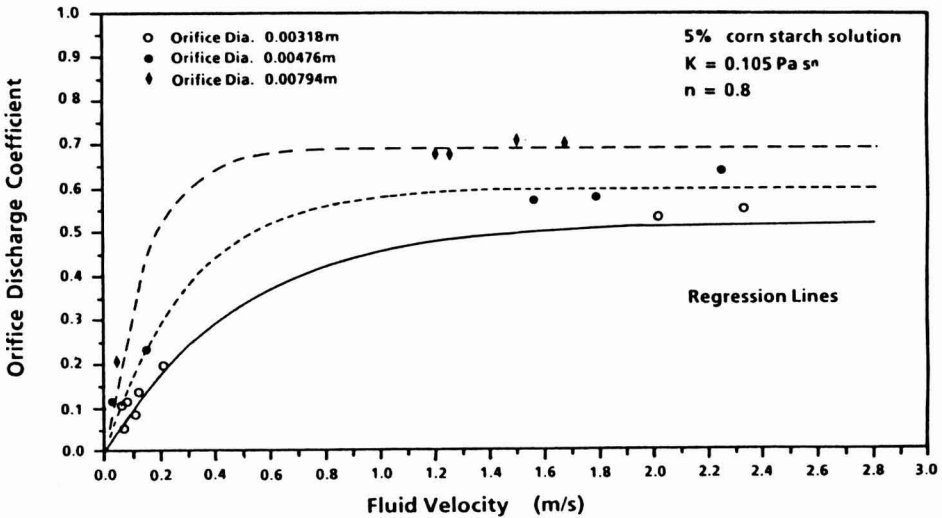
FIGURE 3.

FIG. 3. ORIFICE DISCHARGE COEFFICIENT, AS A FUNCTION OF THE FLUID VELOCITY
IN THE ORIFICE, FOR A 5% AQUEOUS CORN STARCH SOLUTION

The coefficients, β_1 and β_2, were determined (Table 2) by nonlinear regression analysis. A comparison of the experimental data and the regression curves (Fig. 3, 4 and 5) indicates that the experimental orifice discharge coefficients fit well

within the regression line in the range of fluid velocities studied. It should be noted that Eq. (6) does not have any particular physical significance and is presented only as a compact representation of the experimental data.
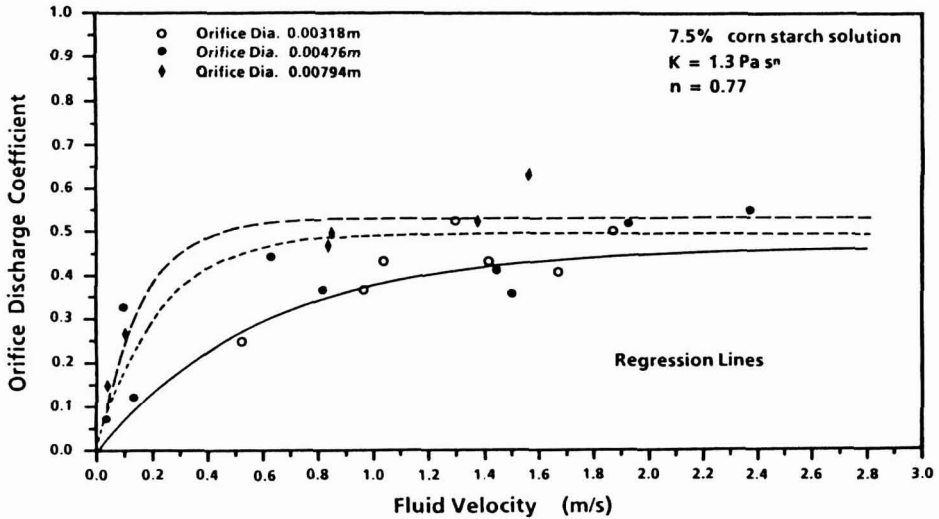
FIGURE 4.

FIG. 4. ORIFICE DISCHARGE COEFFICIENT, AS A FUNCTION OF THE FLUID VELOCITY IN THE ORIFICE, FOR A 7.5% AQUEOUS CORN STARCH SOLUTION
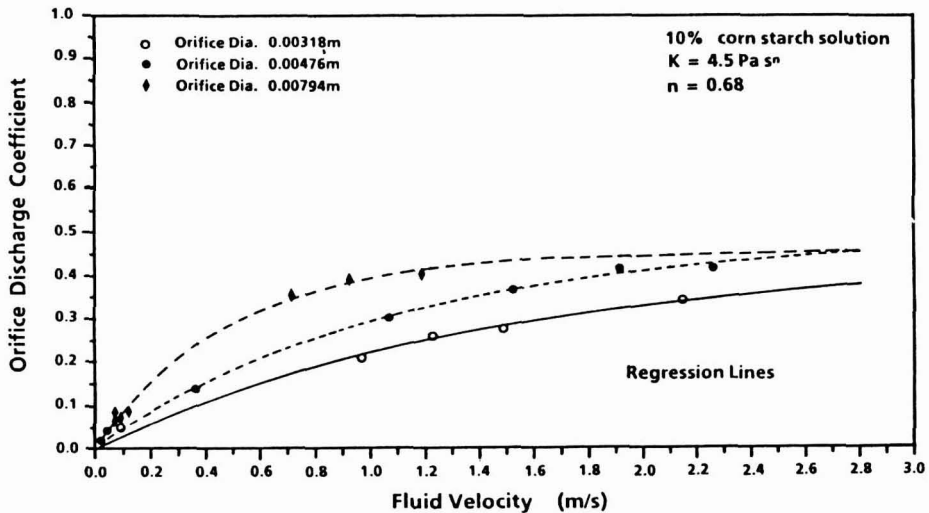
FIGURE 5.

FIG. 5. ORIFICE DISCHARGE COEFFICIENT, AS A FUNCTION OF THE FLUID VELOCITY IN THE ORIFICE, FOR A 10.0% AQUEOUS CORN STARCH SOLUTION

TABLE 2.
PARAMETERS TO DETERMINE ORIFICE DISCHARGE COEFFICIENTS FOR EQ. (6):

$$C = B_1(1 - \exp(-B_2 v))$$

Starch Solution %	Orifice Diameter m	B_1 dimensionless	B_2 s/m	r^2
5.0	0.00318	0.5188	2.077	0.96
	0.00476	0.5894	3.303	0.98
	0.00794	0.6813	6.944	0.99
7.5	0.00318	0.4636	1.709	0.84
	0.00476	0.4863	4.638	0.81
	0.00794	0.5219	6.326	0.90
10.0	0.00318	0.4229	0.743	0.99
	0.00476	0.4308	0.881	0.99
	0.00794	0.4398	2.019	0.99
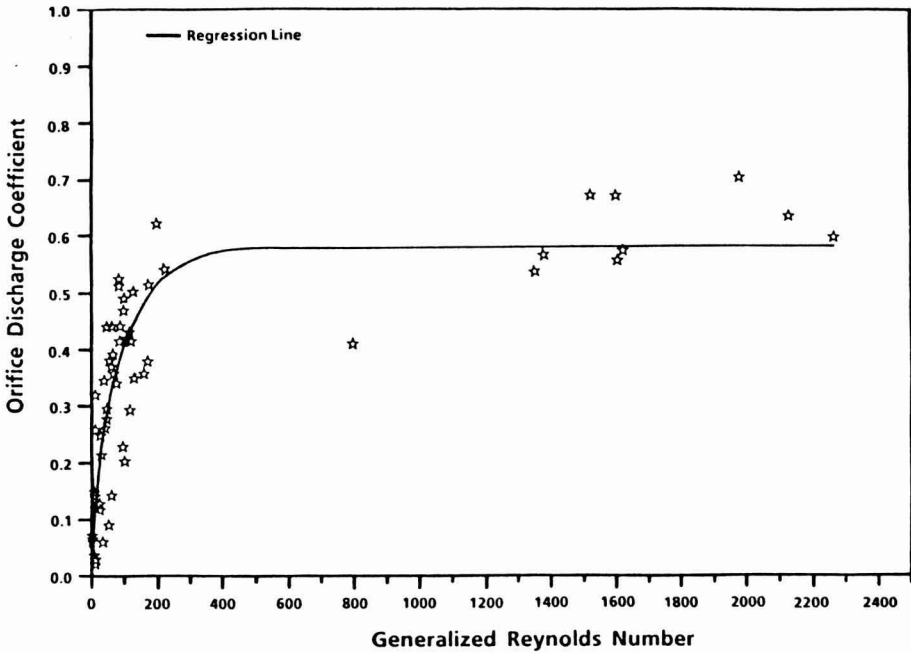
FIG. 6. ORIFICE DISCHARGE COEFFICIENT PRESENTED AS A FUNCTION
OF THE GENERALIZED REYNOLDS NUMBER

Orifice discharge coefficients were also calculated in terms of the generalized Reynolds number, based on the fluid velocity in the orifice:

$$Re = \frac{d^n \rho v^{2-n}}{8^{1-n}K}\left[\frac{4n}{1+3n}\right]^n \tag{7}$$

Using an expression similar to Eq. (6), the mathematical relationship between the discharge coefficient and the generalized Reynolds number was determined:

$$C = 0.494(1 - \exp(-0.011 Re)) + 0.086 \tag{8}$$

Eq. (8) had a correlation coefficient (r^2) equal to 0.77 and represents the best fit of the experimental data. Plotting the results, one can see that most of the Re values are in the laminar region and C values increase with increasing Re values. Equation (8) is very useful because it allows the orifice discharge coefficient to be calculated for any power-law fluid, orifice diameter and orifice fluid velocity. However, the expression should be only considered valid over the range of parameters considered in the present study.

CONCLUSIONS

The orifice discharge coefficient for a non-Newtonian fluid (power-law model) was found to be in the range of 0–0.7. Rheological properties of the fluid (consistency coefficient and flow behavior index) and the orifice diameter strongly influence the orifice discharge coefficient at low fluid velocities: at high velocities, constant values are obtained. The orifice discharge coefficient may be expressed as an exponential function of the generalized Reynolds number calculated in terms of the fluid velocity in the orifice.

NOMENCLATURE

A = cross-sectional area of the orifice, m²
B_1 = constant defined by Eq. (6), dimensionless
B_2 = constant defined by Eq. (6), s/m
C = orifice discharge coefficient, dimensionless
d = orifice diameter, m
g = gravitational acceleration, 9.81 m/s²
K_0 = consistency coefficient, Pa s^n
k_0 = orifice friction loss coefficient, dimensionless
n = flow behavior index, dimensionless
p = pressure, Pa
q = mass flow rate at the orifice, kg/s

Re = generalized Reynolds number in orifice, dimensionless
v = bulk or average velocity, m/s
z = elevation above a reference point, m
α = kinetic energy coefficient, dimensionless
ϱ = fluid density, kg/m^3

REFERENCES

DeCARLO, J.P. 1984, *Fundamentals of Flow Management*. Publishers Creative Services, North Carolina.

KRIEGER, I.M. 1968. Shear rate in a couette viscometer. Trans. Soc. Rheology *12*, 5–11.

OSORIO, F.A. and STEFFE, J.F. 1984. Kinetic energy calculation for non-Newtonian fluids in circular tubes. J. of Food Sci. *49*, 1295–1296, 1315.

PERRY, R.H. and GREEN, D.W. and MALONEY, J.O. 1984. *Chemical Engineers' Handbook*, Sixth Edition. McGraw-Hill Book Co., New York.

VENNARD, J.K. and STREET, R.L. 1975. *Elementary Fluid Mechanics*. John Wiley & Sons, New York.

WHORLOW, R.W. 1980. *Rheological Techniques*. Halsted Press, New York.

THE COMPACTION PROPERTIES OF DEHYDRATED POTATO

J.M. FERDINAND, A.R. KIRBY and A.C. SMITH[1]

AFRC Institute of Food Research,
Norwich Laboratory
Colney Lane,
Norwich, NR4 7UA

ABSTRACT

The compaction behavior of two dehydrated potato granule materials has been studied in a cylindrical geometry. The effect of moisture content and the addition of dehydrated potato flake and potato starches has also been considered. The coefficient of friction and the stress anisotropy factor have been calculated from the pressure transmission measurements using a semi-particulate analysis previously used for polymer powders. The two granule types behaved more similarly under those conditions than their Brabender consistencies implied. The stress anisotropy factor tended to unity with increasing moisture content. The presence of other potato materials had a considerable effect on the compaction of the granules. These results indicate that the performance of processes that involve compaction of these materials, such as extrusion, will vary considerably with composition and moisture content.

INTRODUCTION

Dehydrated potato is a major raw material in the production of snack food products using extrusion and sheet and cut processes. Studies of dehydrated potato have emphasized the microstructural differences of materials produced by different preparation routes rather than their processing performance (Jadhav *et al.* 1976; Reinders 1976; Crum 1976). Dehydrated potato is often characterized using water binding capacity, iodine blue values, particle size distributions and various rheological techniques such as Brabender viscoamylography. The Brabender viscoamylograph is a rheological test which gives a characteristic torque-time response from which the initial and the final values are extracted (Reinders 1976; Crum 1976). Similar information may be obtained in rheological units using proprietary rheometers such as those using the Couette

geometry. The shear viscosity may then be obtained for dilute dispersions as a function of shear rate, temperature and thermal history. Recently the shear viscosity of 9.1% (by weight) dispersions of potato granules in water was obtained as a function of shear rate before and after heating at 80 °C for 15 min. The response was compared with potato starch and pregelatinized starch (Senouci and Smith 1986), two other materials used in potato forming processes.

Extrusion and other processes employing dehydrated potato are usually carried out with a low level of added water. Therefore, although the Brabender technique and dilute rheological measurements differentiate between raw materials, it remains questionable whether these results are applicable to low moisture systems. The rheological properties of low moisture food materials have been obtained using capillary rheometry (Remsen and Clark 1978; Jao et al. 1978; Jasberg et al. 1981; Senouci et al. 1988) and extruder-fed dies (Harper et al. 1971; Van Zuilichem et al. 1980; Fletcher et al. 1985) although these data are generally obtained at elevated temperatures. Recently the shear and extensional rheologies of dehydrated potato granules have been obtained using these approaches (Senouci and Smith 1988). The relevance of low temperature rheological measurements in understanding the effect of raw material variations on extrusion behavior has recently been demonstrated (Ferdinand et al. 1989). Differences in the response of potato granule types singly and in mixtures with pregelatinized potato starch were observed at 25 °C, but not at 80 °C. This accorded with extruder response where pressure differences were observed to be more marked in the first (low temperature) section of the barrel.

Capillary rheometer experiments are not always possible at low moistures and low temperatures. A compaction experiment is particularly suited to the assessment of the rheological properties of low moisture food materials. For example, the compaction response of maize flour has also been reported as a function of moisture content and compaction rate (Briscoe et al. 1987).

This paper analyzes the compaction experiment to obtain the coefficient of friction and stress transmission anisotropy of different potato granule types singly and in mixtures with potato starch and potato flakes. These basic physical data are applicable to low moisture compaction, feeding and extrusion systems and complement studies on the viscous flow properties.

MATERIALS AND METHODS

Materials

The potato materials used were:
(1) Potato granules - Commercial materials differentiated here by the letters A and B. They had Brabender values of 328 and 1075, respectively, and were identical with respect to reducing sugar and monoglyceride levels.

(2)   Potato flake (PF) - (Commercial material)
(3)   Potato starch (PS) - (Tunnel Avebe Farina)
(3)   Pregelatinized potato starch (PPS) - (Tunnel Avebe Paselli WA4).

Different moisture contents expressed on a wet weight basis (w.w.b.) were obtained by mixing these materials by hand with distilled water for 20 min.

Methods

A compaction apparatus was constructed by adapting a capillary rheometer (Carter Baker Enterprises). The rheometer comprised a heated barrel reservoir which was filled with a known height of material. A piston of radius 25 mm was driven vertically at constant speed (5 mm min^{-1}) and the axial loads measured by transducers above the piston and below the material (Fig. 1). A pressure probe (Gentran 3000 p.s.i.) was located 17mm from the lower load cell to measure the radial pressure, P_R. The loads and pressure were monitored continuously using a microcomputer data acquisition system. The applied, P_A, and transmitted P_T, axial pressures were derived from the load cell readings and the cross sectional area of the barrel.

These pressures were measured as a function of the height of material in the barrel, H, for initial heights, Ho, from 34 to 110mm. The experiments were carried out with potato granules A and B for moisture contents in the range 10 to 30% (w.w.b.) and for potato granule B mixed with 10, 20 or 30% of PF, PS or PPS at moisture contents of 10, 23 and 30% (w.w.b.). PF, PS and PPS were also studied separately at 10% moisture (w.w.b.).

Results are given as an average of six measurements for each experimental condition.

THEORY

The classical analyses of compaction have been reviewed by Nedderman (1982). For a cylindrical geometry the Janssen-slice method has been used in a number of studies. Here the treatment of Isherwood and Katwiremu (1982) is reproduced. A Janssen differential slice is shown in Fig. 2 which gives the stresses acting on the material. A force balance yields

$$\pi R^2 . dp = 2 \pi R \tau dz \qquad (1)$$

where p is the axial pressure, R is the cylinder radius and τ is the shear strength of the material at the wall.

$$\tau = \mu p_R$$

where μ is the coefficient of friction and p_R is the radial pressure.
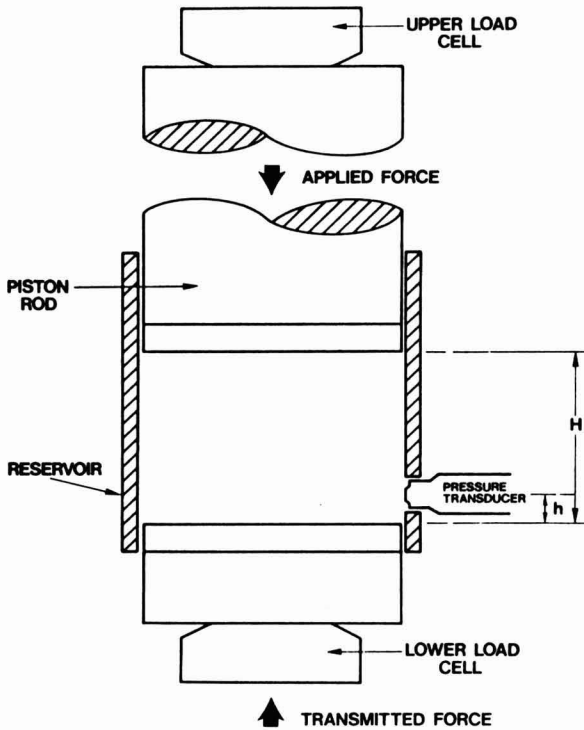
FIG. 1. SCHEMATIC DIAGRAM OF THE COMPACTION EXPERIMENT

A stress anistropy coefficient α is introduced where

$$P_R = \alpha p$$

By substitution equation (1) becomes

$$\pi R^2 \, dp = 2 \pi R \mu \alpha \, p \, dz$$

Integrating over a height H gives

$$\int_0^H 2\mu\alpha \, \frac{dz}{R} = \int_{P_T}^{P_A} \frac{dp}{p} \qquad (2)$$

where $p = P_A$ at $z = H$ and $p = P_T$ at $z = 0$

$$P_A = P_T \exp\left(2\mu\alpha \, \frac{H}{R} \right) \qquad (3)$$

This treatment neglects the variation of the coefficient of friction with normal stress and the contact mechanics of the particles at the wall (Briscoe *et al.* 1985, 1987).
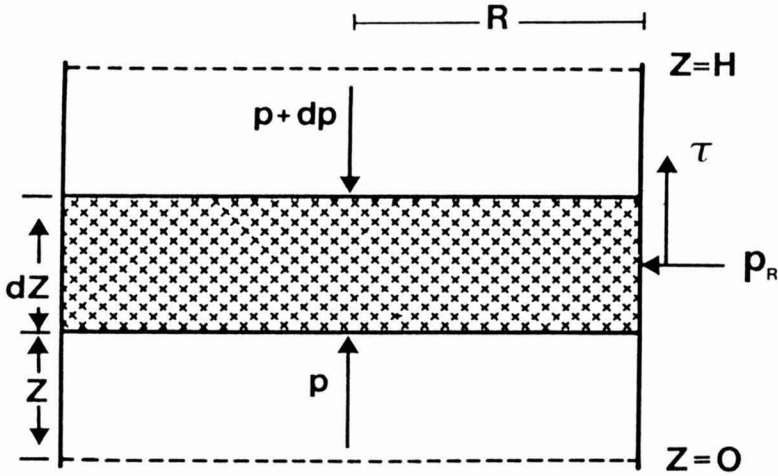
FIG. 2. JANSSEN SLICE DESCRIPTION OF AN ELEMENT OF MATERIAL
IN THE CYLINDER

R   Radius of cylinder
p   axial pressure
P_R radial pressure
H   compact height
τ Shear stress at the wall

Isherwood and Katwiremu (1982) commented that Eq. (3) was physically
unrealistic since the ratio P_T/P_A remained constant experimentally as H varied.
The derivation of Eq. (3) is based on a continuum approach. A semi-particulate
approach leads to an equation similar to Eq. (2). It follows the argument that
there are n_0 particles per unit area at any section. In compaction the number of
particles per unit area in the axial direction increases to some value n. There was
assumed to be no change in any other direction.

The total axial force, F, at z is given by

$$F = n_0 \, \pi R^2 \, f_z$$

where f_z is the axial force per particle and

$$dF = n_0 \, \pi R^2 \, df_z$$

The frictional resistance in the increment dz is

$$2 n f_r \, \pi R \, dz$$

where f_r is the radial contact force per particle. A force balance following similar
arguments to the continuum approach gives

$$n_0 \, \pi R^2 \, df_z = 2 \, n\alpha\mu \, f_z \, dz$$

In terms of axial pressure

$$n_0 \, \pi R^2 \, dp = 2n\alpha\mu \, pdz$$

Integrating as before (Eq. 2)

$$\int_0^H \frac{2\mu\alpha}{R} \frac{n}{n_o} dz \quad = \quad \int_{P_T}^{P_A} \frac{dp}{p}$$

and

$$\int_0^H n\,dz \;=\; n_o H_o$$

since the number of particles in the compact remains constant.

Hence $$P_A \;=\; P_T \exp\left(\frac{2\mu\alpha\,H_o}{R}\right) \tag{4}$$

which may be compared with Eq. (3).

For an initial height H_o^1 of material, the transmitted pressure P_T^1 is given by

$$P_A \;=\; P_T^1 \exp\left(\frac{2\mu\alpha\,H_o^1}{R}\right).$$

The radial pressure at this point P_R is given by

$$P_A \;=\; \frac{1}{\alpha} P_R \exp\left(\frac{2\mu\alpha\,H_o^1}{R}\right) \tag{5}$$

Equations (4) and (5) may be solved for μ and α for the case where $H_o^1 = H_o -$ h where h is the axial distance between the transmission load cell and the radial pressure transducer (Fig. 1).

RESULTS AND DISCUSSION

The transmitted pressure deviated from Eq. (3) as shown earlier for polymer powders (Isherwood and Katwiremu 1982). The logarithm of the applied pressure relative to the transmitted pressure was plotted against displacement, H in Fig. 3. The pressure ratio was almost constant as a function of the compact height H but varied with the initial height H_o. Figure 4 shows the logarithm of the applied pressure relative to the transmitted pressure under equilibrium conditions (after some 20mm displacement of the piston) as a function of the initial height H_o. These data indicate that Eq. 4 provides the better description of the compaction experiment results. The semi-particulate analysis was therefore, used as the basis for the present calculations.
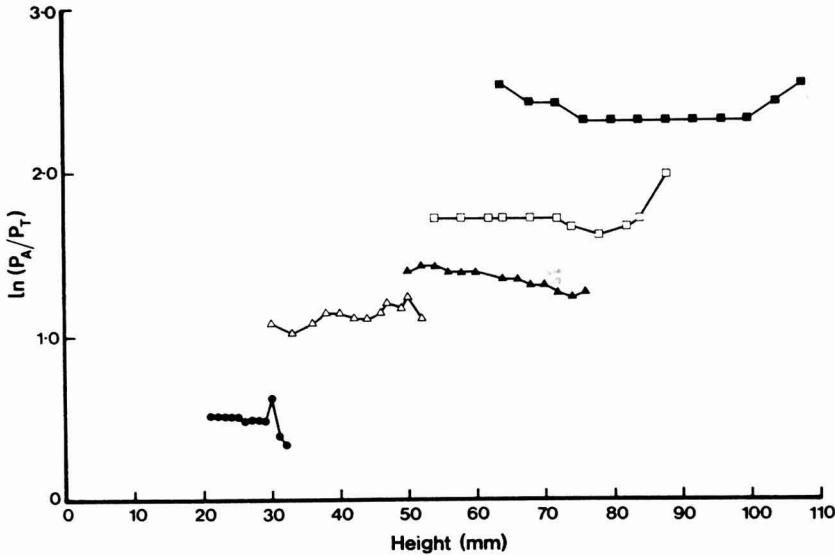
FIG. 3. THE LOGARITHM OF THE RATIO OF APPLIED TO TRANSMITTED PRESSURES (P_A/P_T) AS A FUNCTION OF THE COMPACT HEIGHT H FOR DIFFERENT INITIAL HEIGHTS, H_0, OF GRANULE B AT 10% MOISTURE CONTENT (WET WEIGHT BASIS)

	H_0(mm)
●	34
△	55
▲	80
□	91
■	110

The simultaneous solution of Eq. 4 and 5 provides estimates of the parameters α and μ. The standard deviation was less than 8%. Their variation with moisture content is shown in Fig. 5 for both potato granules. The value of α tended to unity with increasing moisture as the system became more mobile and the stress state tended to hydrostatic. The variation of μ was more complex. The decrease of μ at the highest moisture was consistent with the viscosity of food doughs which decreased with increasing moisture content (Harper *et al.* 1971; Remsen and Clark 1978).

The effect of starch or flake addition level on μ and α of the potato granules depended on the moisture content. At a moisture content of 23% (w.w.b.) μ decreased with increasing proportion of the second material whereas at the highest moisture of study (30% w.w.b.) μ increased (Fig. 6 and 7). The value of μ was almost constant for 10% (w.w.b.) moisture mixes (Fig. 8). The value of α was generally constant for additive levels of 10 to 30% for each moisture content. The greatest change in α occurred between the pure granule and the mixture incorporating a 10% level of starch or flake.
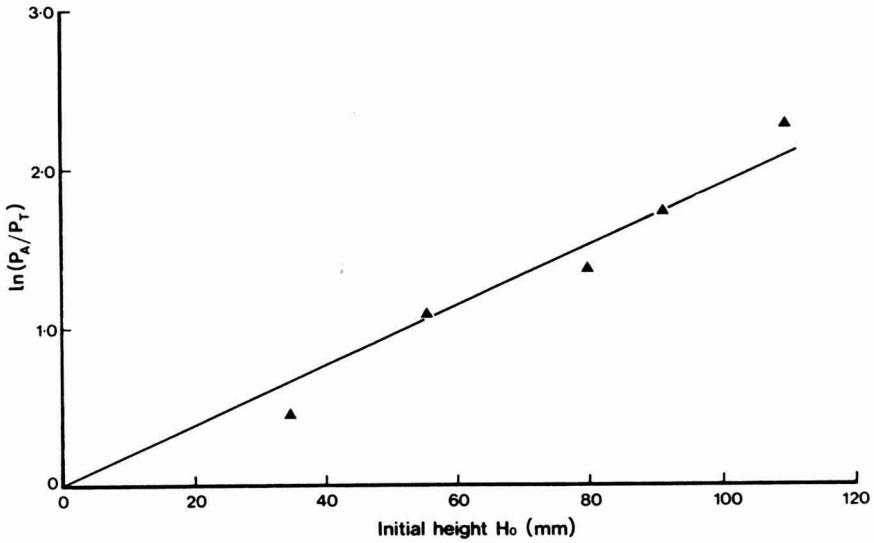
FIG. 4. THE LOGARITHM OF THE RATIO OF APPLIED TO TRANSMITTED PRESSURES
(P_A/P_T) AS A FUNCTION OF THE INITIAL HEIGHT, H_o, FOR GRANULE B
Moisture content = 10% (wet weight basis)
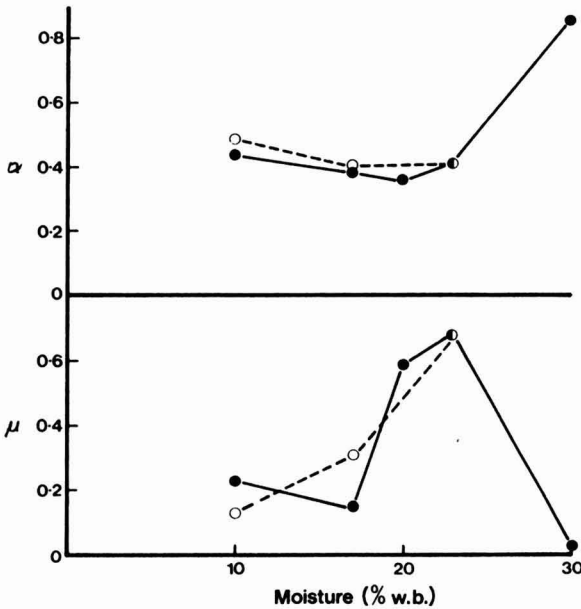
FIG. 5. THE FRICTION COEFFICIENT, μ, AND THE STRESS TRANSMISSION
COEFFICIENT, α AS A FUNCTION OF MOISTURE CONTENT (% W.B., WET WEIGHT
BASIS) FOR POTATO GRANULES A($\bigcirc$) AND B ($\bullet$)

FIG. 6. THE FRICTION COEFFICIENT, μ, AND THE STRESS TRANSMISSION
COEFFICIENT, α, AS A FUNCTION OF ADDITIVE LEVEL FOR A MOISTURE CONTENT
OF 23% (WET WEIGHT BASIS)

a) granule A   b) granule B
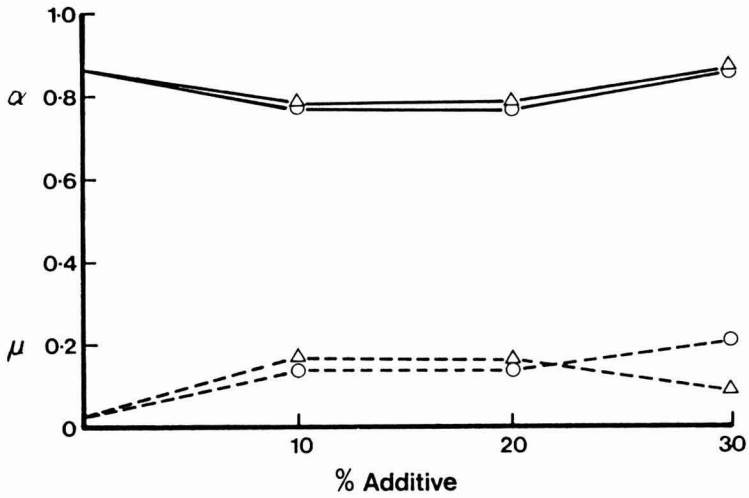
Additives: ○ PS;   △ PF;   □ PPS.

FIG. 7. THE FRICTION COEFFICIENT, μ, AND THE STRESS TRANSMISSION COEFFI-
CIENT, α, AS A FUNCTION OF ADDITIVE LEVEL FOR A MOISTURE CONTENT OF 30%
(WET WEIGHT BASIS) FOR GRANULE B

μ _ _ _ _ α_____
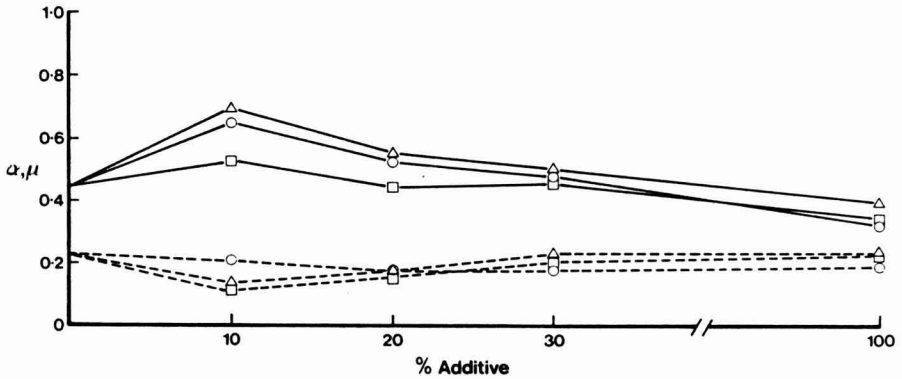
Additives: ○ PS;   Δ PF.

FIG. 8. THE FRICTION COEFFICIENT, μ, AND THE STRESS TRANSMISSION
COEFFICIENT, α, AS A FUNCTION OF ADDITIVE LEVEL FOR A MOISTURE CONTENT
OF 10% (WET WEIGHT BASIS) FOR GRANULE B

μ _ _ _ _ α_____

Additives: ○ PS;   Δ PF.   □ PPS.

The results of some previous studies using the Janssen treatment are summarized in Table 1. The angle of internal friction, ϕ_i has also been measured for a number of food systems. The Janssen analysis provides a lower bound expression for α in terms of ϕ_i.

$$1 \geqslant \alpha \geqslant \frac{1 - \sin \phi_i}{1 + \sin \phi_i}$$

Values of ϕ_i and the corresponding values of α are also recorded in Table 1. In the present work $\alpha = 0.33$ for potato starch at 10% (w.w.b.) moisture compared to lower bound values in the range 0.25–0.33 obtained by Peleg et al. (1973) and Mannheim and Passy (1982) for moistures from 2 to 15%.

TABLE 1.
VALUES OF α, μ and ϕ_i CITED IN THE LITERATURE FOR FOOD MATERIALS

	α	μ	ϕ_i	Reference
Wheat	0.64	0.37	–	Sundaram and Cowin
Shelled corn	0.72	0.34	–	"
Soy beans	0.40	0.54	–	"
Soybean meal	0.44	–	–	Clower et al
Corn meal	0.50	–	–	"
Wheat	0.52	–	–	"
Sugar beet pulp	0.59	–	–	"
Corn starch	0.26–0.32	–	31–36	Peleg et al
Potato starch	0.25	–	37	"
Potato starch	0.27–0.33	–	30–35	Mannheim and Passy

It follows from Eq. 4 and 5 that the pressure transmission in a compacting powder depended on the coefficient of friction μ and the stress anistropy ratio, α, which in turn varied with moisture content and composition. Classical treatments of the feed zone of single screw extruders depend on the coefficient of friction (Tadmor and Klein 1970). Flood fed extruders require an analysis of the

type given in Eq. 4 and 5 to predict the pressure at the base of the feed hopper. Briscoe *et al.* (1987) have shown that the pressure rise in a single screw extruder feed zone through traction-induced compaction may be described by the uniaxial compaction equations. The pressure increases exponentially with the product of μ and α. In a qualitative manner the pressure in the feed zone would be correlated with these powder parameters. This is illustrated in Table 2 from experiments described more fully elsewhere (Ferdinand *et al* 1989). It is also evident that the two granules considered here were less different than their Brabender values implied.

TABLE 2.
PRESSURE GENERATION IN THE FEED ZONE
OF A STARVE-FED SINGLE SCREW EXTRUDER

Feed material	Moisture content (% w.w.b.)	$\mu\alpha$	Feed zone pressure[*] (MPa)
Potato granule A	23	0.28	7.3
Potato granule B	23	0.28	6.8
Potato granule B + 30% PF	30	0.08	2.2
Potato granule A + 30% PF	23	0.24	3.1

*Extrusion using an Almex screw extruder with a compression of 3:1, one circular die of diameter 4 mm, feed rate = 28 kg h^{-1}, screw speed = 80 rpm, set barrel temperature = 25 °C. Pressure measurement point 430 mm from center of feed port.

CONCLUSIONS

A compaction technique was used to obtain the pressure transmission properties of potato starch materials singly and in mixtures. The data presented in this paper are applicable to commercial food materials and are required in models of compaction and conveying processes. The results were in agreement with a semi-particulate analysis which has been used for polymer powders.

Considerable variations in the coefficient of friction and stress anisotropy coefficient of potato granules occurred as a function of moisture content and with the addition of potato starch, pregelatinized potato starch or potato flake. The coefficient of friction varied by at least a factor of ten for potato granules in the moisture content range 10 to 30% (w.w.b.). The stress anistropy coefficient for potato starch was in agreement with the literature value obtained by a different approach.

ACKNOWLEDGMENT

REFERENCES

BRISCOE, B.J., FERNANDO, M.S.D. and SMITH, A.C. 1985. The interfacial friction of compacted maize powders. J. Phys. D: Appl. Phys. *18*, 1069–1085.

BRISCOE, B.J., FERNANDO, M.S.D. and SMITH, A.C. 1987. The role of interfacial friction in the compaction of maize. In *Tribology in Particle Technology*, (B.J. Briscoe and M.J. Adams, eds.) pp. 220–233, Adam Hilger, Bristol.

CLOWER, R.E., ROSS, I.J. and WHITE, G.M. 1973. Properties of compressible granular materials as related to forces in bulk storage structures. Trans. A.S.A.E. *16*, 478–481.

CRUM, M.G. 1976. Developments and manufacturing of starch based snacks and confectionery products by direct extrusion cooking. pp. 25–41, Proc. International Snack Seminar, Solingen, W. Germany.

FERDINAND, J.M., KIRBY, A.R. and SMITH, A.C. 1989. The extrusion rheology of dehydrated potato. J. Food Eng. *10*, 73–80.

FLETCHER, S.I., McMASTER, T.J., RICHMOND, P. and SMITH, A.C. 1985. Rheology and extrusion of maize grits. Chem. Eng. Comm. *32*, 239–262.

HARPER, J.M., RHODES, T.P. and WANNINGER, L.A. 1971. Viscosity model for cooked cereal doughs. Chem. Eng. Prog. Symp. Series. *67*, 40–43.

ISHERWOOD, D.P. and KATWIREMU, J.B. 1982. Effect of die wall friction on the compaction of polymer particles. Plastics Rubber Proc. Appl. *2*, 253–263.

JADHAV, S.J., BERRY, L.M. and CLEGG, L.F.L. 1976. Extruded french fries from dehydrated potato granules processed by a freeze-thaw technique. J. Food Sci. *41*, 852–855.

JAO, Y.C., CHEN, A.H., LEWANDOWSKI, D. and IRWIN, W.E. 1978. Engineering analysis of soy dough rheology in extrusion. J. Food Proc. Eng. 2, 97–112.

JASBERG, B.K., MUSTAKAS, G.C. and BAGLEY, E.B. 1981. Effect of extruder retention time on capillary flow of soy dough. J. Food Proc. Eng. 5, 43–56.

MANNHEIM, C.H. and PASSY, N. 1982. Flow properties and water sorption of food powders I. Starches. Lebensm-Wiss. u-Technol. 15, 216–221

NEDDERMAN, R.M. 1982. The theoretical prediction of stress distributions in hoppers. Trans. I. Chem. E. 60, 259–275.

PELEG, M., MANNHEIM, C.H. and PASSY, N. 1973. Flow properties of some food powders. J. Food Sci. 38, 959–964.

REINDERS, M.A. 1976. General survey of starch based ingredients in the direct extrusion cooking process. pp. 3–22, Proc. International Snack Seminar. Solingen, W. Germany.

REMSEN, C.H. and CLARK, J.P. 1978. A viscosity model for a cooking dough. J. Food Proc. Eng. 2, 39–64.

SENOUCI, A. and SMITH, A.C. 1986. The extrusion cooking of potato starch material. Die Starke, 38, 78–82.

SENOUCI, A., SIODLAK, G.D.E. and SMITH, A.C. 1988. Extensional rheology in food processing. In Progress and Trends in Rheology II, (H. Giesekus and M.F. Hibberd, eds.) pp. 434–437, Steinkopff Verlag, Darmstadt.

SENOUCI, A. and SMITH, A.C. 1988. An experimental study of food melt rheology. Rheol. Acta. 27, 546–554, 649–655.

SUNDARAM, V. and COWIN, S.C. 1979. A reassessment of static bin pressure experiments. Powder Technol. 22, 23–32.

TADMOR, Z. and KLEIN, I. 1970. The Principles of Plasticating Extrusion, pp. 49–77, Van Nostrand Rheinhold, New York.

VAN ZUILICHEM, D.J., BRUIN, S., JANSSEN, L.F.B.M. and STOLP, W. 1980. Single screw extrusion of starch and protein-rich materials. In Food Process Engineering, Vol. 1, Food Processing Systems, (P. Linko, Y. Malkki, J. Olkku and J. Larinkari, eds.) pp. 745–756, Applied Science, London.

ON THE DESIGN OF TRIPLE CONCENTRIC-TUBE HEAT EXCHANGERS[1]

CARLOS A. ZURITZ

Department of Agricultural Engineering
The Pennsylvania State University
225 Agricultural Engineering Bldg.
University Park, PA 16802

ABSTRACT

A set of analytical equations for a triple-tube heat exchanger was developed. They allow for independent computations of bulk (cross-sectional area averaged) fluid temperatures at any axial location along the heat exchanger and are valid for parallel and counter flow configurations. The equations account for heat losses to the surroundings and are useful for design purposes. Mass flow rates, inlet fluid temperatures and heat transfer coefficients are input parameters required for temperature calculations. A simplified approximate equation for total rate of heat transfer, in terms of logarithmic mean temperature differences, was derived for well-insulated heat exchangers and tested with the analytical equations. A case study is presented and the computational procedure is discussed. Results obtained with the simplified total rate of heat transfer equation were in excellent agreement with those obtained with the analytical equations. Simulations show that the creation of an annular region within the inner pipe increases the overall heat transfer efficiency and reduces the heat exchanger length requirement by almost 25%.

INTRODUCTION

One of the most important engineering design problems in process heat transfer involves the exchange of heat between two or more streams of fluids. A considerable amount of research has been devoted to the subject of heat exchangers and much heat transfer data and correlations are available in the literature. Books entirely devoted to the subject of heat exchangers have been published (Kays 1964; Spalding and Taborek 1983).

Indirect-contact heat exchangers are by far the most widely used equipment in processes involving the transfer of heat. The simplest of such equipment is the double-pipe heat exchanger. More space efficient equipment are the shell-and-tube and the plate heat exchangers. A major characteristic of heat exchanger design is the relative flow configuration. The more common configurations are counter flow, parallel flow, cross flow, cross-counter flow and multipass shell and tube.

Triple concentric-tube heat exchangers are an improved version of the double-pipe exchanger. The main improvements include a larger area per unit length available for heat transfer and better overall heat transfer coefficients due to higher fluid velocities in the annular regions. Several commercial models are available and in use in the food industry. New models with more than three concentric tubes have been developed with heat transfer efficiencies comparable to plate heat exchangers and with the added advantages that they can handle liquids with susupended solids and do not present the problem of leaking gaskets. Although concentric-tube heat exchangers can present a problem with regard to cleaning of the heat transfer surfaces, cartridge type multiple-tube heat exchangers have been developed which operate with minimum fouling and can be quickly disassembled and cleaned, Margittai (1982); North and Bacchetti (1983).

Despite the large number of design equations for different types of heat exchangers available in the literature, no analytical equations have been developed to predict temperature distributions in multiple concentric-tube heat exchangers.

The objective of this paper is to develop a set of design expressions for computation of fluid stream temperatures in a triple concentric-tube heat exchanger.

MATHEMATICAL FORMULATION

A triple-tube heat exchanger is shown in Fig. 1 for a counter-current flow configuration. The heating medium flows through the inner tube and the outermost annulus, and the product through the center annulus in the opposite direction. For a steady process, the macroscopic thermal energy balance applied to each of the control volumes shown in Fig. 1, in differential form in the z-direction, yields:

$$- dq_{IIo} - dq_{IIi} = (MC_p)_I \, dT^I \tag{1}$$

$$- dq_L - dq_{IIo} = (MC_p)_{IIo} dT^{IIo} \tag{2}$$

$$- dq_{IIi} = (MC_p)_{IIi} dT^{IIi} \tag{3}$$
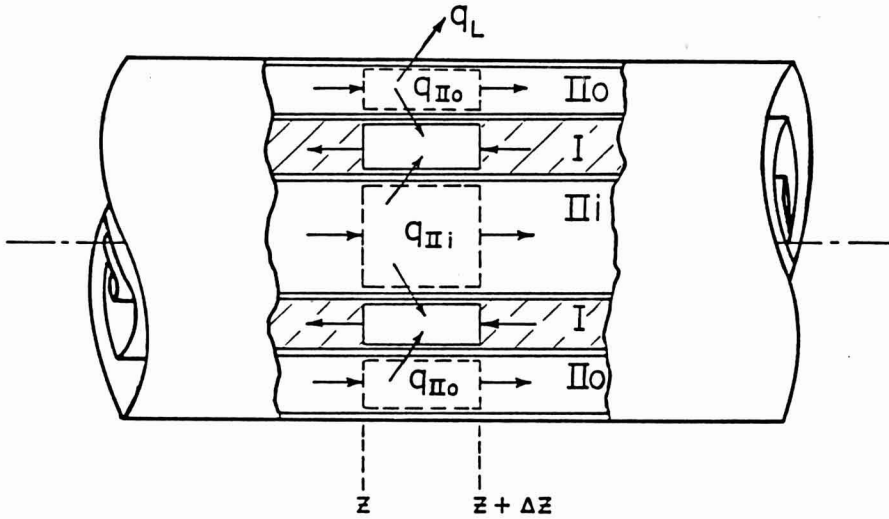
FIG. 1. CONTROL VOLUMES FOR ENERGY BALANCES
IN A COUNTER-CURRENT TRIPLE-TUBE HEAT EXCHANGER

Where the heat transfer rates are expressed as

$$dq_{IIo} = U_o P_o (T^{IIo} - T^I) \, dz \tag{4}$$

$$dq_{IIi} = U_i P_i (T^{IIi} - T^I) \, dz \tag{5}$$

$$dq_L = U_L P_L (T^{IIo} - T_a) \, dz \tag{6}$$

Substitution of equations (4) to (6) into (1) to (3) gives

$$\frac{dT^I}{dz} = -\frac{U_o P_o}{(MC_p)_I} (T^{IIo} - T^I) - \frac{U_i P_i}{(MC_p)_I} (T^{IIi} - T^I) \tag{7}$$

$$\frac{dT^{IIo}}{dz} = -\frac{U_o P_o}{(MC_p)_{IIo}} (T^{IIo} - T^I) - \frac{U_L P_L}{(MC_p)_{IIo}} (T^{IIo} - T_a) \tag{8}$$

$$\frac{dT^{IIi}}{dz} = -\frac{U_i P_i}{(MC_p)_{IIi}} (T^{IIi} - T^I) \tag{9}$$

By using the following definitions

$$X_1 = T^I \; ; \; X_2 = T^{IIo} \; ; \; X_3 = T^{IIi}$$

$$\dot{X}_1 = (dT^I/dz) \; ; \; \dot{X}_2 = (dT^{IIo}/dz) \; ; \; \dot{X}_3 = (dT^{IIi}/dz)$$

$$\beta_1 = U_o P_o/(\dot{M}C_p)_I \; ; \; \beta_2 = U_i P_i/(\dot{M}C_p)_I$$

$$\beta_3 = U_o P_o/(\dot{M}C_p)_{IIo}; \; \beta_4 = U_i P_i/(\dot{M}C_p)_{IIi} \tag{12}$$

$$\beta_5 = U_L P_L/(\dot{M}C_p)_{IIo}; \; \beta_6 = U_L P_L T_a/(\dot{M}C_p)_{IIo} \; ; \; or \; \beta_6 = \beta_5 T_a$$

Equations (7) to (9) can be expressed as

$$\dot{X}_1 = (\beta_1 + \beta_2) \; X_1 - \beta_1 X_2 - \beta_2 X_3 \tag{13}$$

$$\dot{X}_2 = \beta_3 X_1 - (\beta_3 + \beta_5) \; X_2 + \beta_6 \tag{14}$$

$$\dot{X}_3 = \beta_4 X_1 - \beta_4 X_3 \tag{15}$$

In order to simplify the mathematical representation, the following definitions are introduced:

$$a_{11} = (\beta_1 + \beta_2); \; a_{12} = -\beta_1; \; a_{13} = -\beta_2; \; a_{14} = 0$$

$$a_{21} = \beta_3; \; a_{22} = -(\beta_3 + \beta_5); \; a_{23} = 0; \; a_{24} = \beta_6 \tag{16a}$$

$$a_{31} = \beta_4; \; a_{32} = 0; \; a_{33} = -\beta_4; \; a_{34} = 0$$

For co-current flow configuration one must change the sign of the coefficients in the first row of Eq. (16a) to:

$$a_{11} = -(\beta_1 + \beta_2); \quad a_{12} = \beta_1; \quad a_{13} = \beta_2 \tag{16b}$$

The other terms remain unchanged. Equations (16a) and (16b) are valid for both heating and cooling modes.

Introducing Eq. (16a) into (13) to (15) gives

$$\dot{X}_1 = a_{11}X_1 + a_{12}X_2 + a_{13}X_3 \tag{17}$$

$$\dot{X}_2 = a_{21}X_1 + a_{22}X_2 + a_{24} \tag{18}$$

$$\dot{X}_3 = a_{31}X_1 + a_{33}X_3 \tag{19}$$

Applying Laplace Transform to Eq. (17) to (19) yields

$$\bar{X}_{1(s)}(s-a_{11}) = X_{1(o)} + a_{12}\bar{X}_{2(s)} + a_{13}\bar{X}_{3(s)} \tag{20}$$

$$\bar{X}_{2(s)}(s-a_{22}) = X_{2(o)} + a_{21}\bar{X}_{1(s)} + a_{24}/s \tag{21}$$

$$\bar{X}_{3(s)}(s-a_{33}) = X_{3(o)} + a_{31}\bar{X}_{1(s)} \tag{22}$$

The solutions of Eq. (20) to (22) are expressed as

$$X_{j(z)} = \sum_{i=1}^{3} \{X_{i(o)}[A_{ij} + B_{ij}\exp(\lambda_1 z) + C_{ij}\exp(\lambda_2 z)]\}$$

$$+ a_{24}[A_{4j}z + B_{4j} + C_{4j}\exp(\lambda_1 z) + D_{4j}\exp(\lambda_2 z)] \tag{23}$$

for j = 1, 2, 3

Since the inlet temperature of the heating/cooling medium is the same in both streams, that is $T_{(o)}^{IIo} = T_{(o)}^{IIi}$ or $X_{2(o)} = X_{3(o)}$, the summation in Eq. (23) can be reduced to two terms, i.e., i = 1,2

$$X_{j(z)} = \sum_{i=1}^{2} \{X_{i(o)}[A_{ij} + B_{ij}\exp(\lambda_1 z) + C_{ij}\exp(\lambda_2 z)]\}$$

$$+ a_{24}[A_{4j}z + B_{4j} + C_{4j}\exp(\lambda_1 z) + D_{4j}\exp(\lambda_2 z)] \tag{24}$$

for j = 1, 2, 3

The constants, A_{ij}, B_{ij}, C_{ij}, A_{4j}, B_{4j}, C_{4j}, and D_{4j}, and roots λ's are given in the Appendix.

Equation (24) allows for the computation of the bulk temperatures $T^I = X_{1(z)}$, $T^{IIo} = X_{2(z)}$ and $T^{IIi} = X_{3(z)}$ at any location along the length of the heat exchanger as a function of inlet temperatures, $(\dot{M}C_p)$'s, overall heat transfer coefficients and perimeters of the concentric tubes. Exit temperatures are obtained from Eq. (24) with $z = L$. In the counter flow configuration, $X_{1(o)}$ represents the product exit temperature which must be evaluated from Eq. (24) for $j = 1$ as a function of $X_{1(L)}$.

Other equations needed for design purposes can be obtained by integrating Eq. (1) to (3) given as

$$Q_T = Q_{IIo} + Q_{IIi} = (\dot{MC}p)_I [T^I_{(o)} - T^I_{(L)}] \tag{25}$$

$$Q_L + Q_{IIo} = (\dot{MC}p)_{IIo} [T^{IIo}_{(o)} - T^{IIo}_{(L)}] \tag{26}$$

$$Q_{IIi} = (\dot{MC}p)_{IIi} [T^{IIi}_{(o)} - T^{IIi}_{(L)}] \tag{27}$$

If the heat exchanger is well insulated, the coefficients β_5 and $\beta_6 (= a_{24})$ can be assumed equal to zero and Eq. (24) reduces to:

$$X_j(z) = \sum_{i=1}^{2} \{X_{1(o)}[A_{1j} + B_{1j}\exp(\lambda_1 z) + C_{1j}\exp(\lambda_2 z)]\} \tag{28}$$

for $j = 1,2,3$

Under this condition $Q_L = o$ and a simplifed, approximate equation for Q_T in terms of the overall heat transfer coefficients and log mean temperature differences can be obtained from Eq. (4), (5) and (25) to (27), by performing a conventional analysis for the individual heat transfer rates Q_{IIo} and Q_{IIi}. The result is expressed as

$$Q_T = U_o A_o \Delta T_{lm_o} + U_i A_i \Delta T_{lm_i} \tag{29}$$

$$\Delta T_{lm_o} = \frac{(T^{IIo} - T^I)_{(L)} - (T^{IIo} - T^I)_{(o)}}{\ln[\frac{(T^{IIo} - T^I)_{(L)}}{(T^{IIo} - T^I)_{(o)}}]} \tag{30}$$

$$\Delta T_{lm_i} = \frac{(T^{IIi}-T^I)_{(L)} - (T^{IIi}-T^I)_{(o)}}{\ln\left[\dfrac{(T^{IIi}-T^I)_{(L)}}{(T^{IIi}-T^I)_{(o)}}\right]} \qquad (31)$$

Where

$$Q_{IIo} = U_o A_o \Delta T_{lm_o} \qquad (32)$$

and

$$Q_{IIi} = U_i A_i \Delta T_{lm_i} \qquad (33)$$

The validity of Eq. (29) to (33) can only be tested with Eq. (26) and (27) after computation of length and exit temperatures with Eq. (28). Although Eq. (25) to (33), for $Q_L = 0$, can be used for design purposes, the computation of unknown parameters is not as straight forward as with other heat exchanger arrangements. In the present case Q_{IIi} and Q_{IIo} can not be solved directly without prior knowledge of $\dot{M}_{IIi}$ and $\dot{M}_{IIo}$ which must be computed based on pressure drop through the heat exchanger. It is also not possible to outline a general computational procedure as it will depend on each particular case. Nevertheless, a case study with a complete computational procedure is presented next. The example requires the calculation of the heat exchanger length by an iterative process using Eq. (28).

CASE STUDY AND COMPUTATIONAL PROCEDURE

A triple-tube heat exchanger is being designed to cool a liquid food from 80 °C to 30 °C. The food product will flow through the center annulus of the heat exchanger at a flow rate of 2000 kg/h. Available cooling water at 15 °C will enter the inner pipe and the outer annulus of the apparatus and flow in counter-current at a total rate of 10000 kg/h. The product physical properties at a bulk average temperature of 55 °C are: density = 1020 kg/m³, specific heat 4.00 kJ/kg °C, thermal conductivity = 0.5 W/m °C and viscosity of 0.0015 Pa-s. The pipe diameters are indicated in Fig. 2 and the dimensions given below. Determine the required length of the heat exchanger and the exit temperatures of the cooling water.
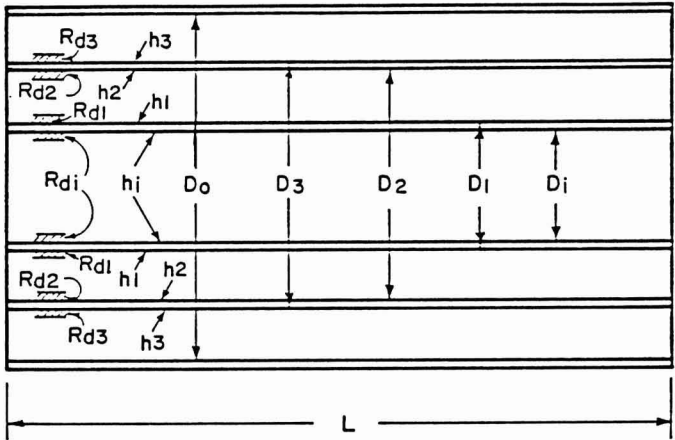
FIG. 2. DEFINITIONS OF DIMENSIONS AND PARAMETERS
IN A TRIPLE-TUBE HEAT EXCHANGER

Pipe Diameters

$$D_i = 0.08 \text{ m} \qquad\qquad D_3 = 0.126 \text{ m}$$

$$D_1 = 0.083 \text{ m} \qquad\qquad D_o = 0.166 \text{ m}$$

$$D_2 = 0.123 \text{ m}$$

The known process conditions are:

$$\dot{M}_I, \ T^I_{(o)}, \ T^I_{(L)}, \ \dot{M}_T = \dot{M}_{IIo} + \dot{M}_{IIIi}, \ T^{IIo}_{(o)} = T^{IIi}_{(o)} \text{ and pipe}$$

diameters.

Figure 2 also indicates the different convective heat transfer coefficients (h's) and fouling factors (Rd's).

A convenient order of calculations is presented below

(1) Determine an average exit bulk temperature of cooling medium from the following equation

$$(\dot{M}C_p)_I \Delta T^I = (\dot{M}C_p)_T \Delta T^T \tag{34}$$

where

$$\Delta T^T = T_{(o)} - T_{(L)},$$

$$T_{(o)} = T^{IIo}_{(o)} = T^{IIi}_{(o)}$$

and

$T_{(L)}$ = average exit bulk temperature of cooling medium

Assume a value for C_{pT} and determine $T_{(L)}$ from Eq. (34) in order to obtain T^Tmean (arithmetic mean bulk temperature of cooling fluid). All other properties (ϱ, μ, k) are determined at the mean temperature.

(2) Determine $\dot{M}_{IIo}$ and $\dot{M}_{IIi}$. Since we are dealing with an annulus and a circular pipe, it is convenient to use an equivalent diameter (De), as defined below:

$$De = 4 \times \text{Cross sectional area/Wetted perimeter} \tag{35}$$

where $D_{eIIi} = D_i$ for pipe and $D_{eIIo} = D_o - D_3$ for annulus.

The ratio $\dot{MR} = \dot{M}_{IIo}/\dot{M}_{IIi}$ can be evaluated by means of any of the available equations relating friction factor (f) to Reynolds number (Re). Using this type of formula requires several iterations and the use of the Moody diagram if f is not an explicit function of Re. If the cooling (or heating) medium is water, Hazen-Williams formula may be used as presented by Streeter and Wylie (1979)

$$f = \frac{1014.2 \, (Re)^{-0.148}}{c^{1.852} D_e^{0.0186}} \qquad \text{, for turbulent flow} \tag{36}$$

or $\qquad f = 16/Re \qquad$, for laminar flow $\tag{37}$

The pressure drop through the central and annular region for the cooling medium is the same (parallel resistance). Therefore, from the definition of pressure drop due to friction, the following relationship can be derived:

$$f_{IIi}/f_{IIo} = (V_{IIo}/V_{IIi})^2 / (D_{eIIo}/D_{eIIi}) \tag{38}$$

For the same flow conditions (either, both laminar or both turbulent) in the outer annulus and the central pipe, the following simplified mass-flow-rate ratios can be derived from Eq. (36) to (38):

For laminar flow

$$\dot{MR} = (\frac{D_{eIIo}}{D_{eIIi}})^4 \tag{39}$$

For turbulent flow

$$\dot{M}R = (\frac{D_{eIIo}}{D_{eIIi}})^{2.63}$$

(40)

Once $\dot{M}R$ is determined, $\dot{M}_{IIIi}$ and $\dot{M}_{IIo}$ are calculated from $\dot{M}R$ and $\dot{M}T$. Next, Re must be calculated to check flow conditions and validity of the selected equation.

(3) The next step involves the computation of the overall heat transfer coefficients. In this case we also use an equivalent diameter (D_e), but for heat transfer the wetted perimeter only involves the area through which this process occurs. Therefore, the D_e used in Re number calculations for heat transfer is different than for pressure drop in annular flow (Kern 1950) and given as

$$D_{eIIo} = (D_o^2 - D_3^2)/D_3$$

(41)

$$D_{eIo} = (D_2^2 - D_1^2)/D_1 \quad ; \quad D_{eIi} = (D_2^2 - D_1^2)/D_2$$

(42)

Each individual heat transfer coefficient can be computed using an appropriate constitutive equation for Nusselt number (Nu), Whitaker (1977), Kern (1950), Heldman and Singh (1981), Perry and Chilton (1973), Jakob (1949), Naughton and Singh (1980). Fouling factors for different fluids and flow conditions are available in the literature, Perry and Chilton (1973), Kern (1950). The overall heat transfer coefficients can then be determined from

$$U_i = \frac{h_i h_1}{[h_1 + h_i \frac{(D_i)}{\overline{D}_1}]} + R_{di} + R_{d1}$$

(43)

$$U_o = \frac{h_2 h_3}{[h_2 + h_3 \frac{(D_3)}{\overline{D}_2}]} + R_{d2} + R_{d3}$$

(44)

where the resistance to heat transfer through the pipe walls has been neglected.

(4) The required length of the heat exchanger (L) can now be determined from Eq. (28) for $j = 1$ and $z = L$. Since L is not explicit, an iterative procedure is required.

(5) Equation (28) can then be used to compute T^{IIo} and T^{IIi} for j = 2 and 3, respectively.

(6) Equations (26), (27), (32), and (33) can be used to adjust the overall heat transfer coefficients U_o and U_i, if needed, and reiterate the computations from step (3). But first, Eq. (32) and (33) need to be tested for validity using the exit temperatures calculated with Eq. (28).

RESULTS AND DISCUSSION

The results presented in Table 1 were obtained following the computational procedure described before. As all the flow conditions were turbulent, the individual flow rates of the cooling medium were computed with Eq. (40) and the total mass flow rate. The convective heat transfer coefficients were calculated from the following Nusselt number correlations:

For flow in pipe

$$Nu = 0.023 \ Re^{0.8} Pr^{1/3} \ (\mu_b/\mu_w)^{0.14}$$

and for flow in annuli

$$Nu = 0.020 \ Re^{0.8} Pr^{1/3} \ (D_2/D_1)^{0.53}$$

The overall heat trasnfer coefficients were calculated with Eq. (43) and (44) neglecting the fouling factors.

The required length (L) calculated with Eq. (28) for j = 1 and z = L was:

$$\text{Required Length (L)} = 34.7 \text{ m}$$

The exit temperatures of the cooling water were also computed with Eq. (28) for j = 2, 3 and z = L, and given in Table 1. They are:

$$T^{IIo} = 39.3\,°C,$$
$$T^{IIi} = 22.2\,°C$$

The required length was recalculated for each individual stream of the cooling water by using Eq. (26), (27), (32) adn (33) with $Q_L = 0$ and the exit temperatures determined with Eq. (28). The results were as follows:

$$L_{IIo} = 33.6 \text{ m}$$
$$L_{IIi} = 35.2 \text{ m}$$

TABLE 1.
RESULTS FOR CASE STUDY

Parameters	Cooling Water		Fluid Food (I)
	Outer Annulus (II_o)	Inner Tube (II_i)	
Mass Flow Rate (kg/hr)	1390	8610	2000
Equivalent Diameter D_e(m) (Heat Transfer)	0.0927	0.08	0.0993 0.0670
Perimeter (m)	0.396	0.251	
Re (Heat Transfer)	5300	38070	4750 7040
Convective Heat Tr. Coeff. (W/m^2°C)	h_3 = 200	h_i = 1520	h_1 = 300 h_2 = 270
Nu	42.30	203.20	49.30 67.50
Overall Heat Tr. Coeff. (W/m^2°C)	U_o = 115	U_i = 256	
Exit Temperatures (°C)	39.3	22.2	30.0
Log Mean Temperature Difference (°C)	25.8	31.7	
Heat Transfer Rates (W)	39,230	71,890	111,120

The above results are in excellent agreement with the length value obtained with Eq. (28). This is an indication that Eq. (29) to (33) are a good approximation and can be used for design purposes.

The results listed in Table 1 indicated that about 86% of the cooling water flowed through the inner pipe giving rise to an overall heat transfer coefficient more than double that for the outer annulus. This resulted in almost twice the rate of heat transfer. A better flow rate distribution would increase the efficiency of the heat exchanger. This could be achieved by inserting a sanitary heat-resistant plastic tube, sealed at the ends, within the inner pipe in order to create an annular region. The improved efficiency would result in a shorter and more economical equipment.

A computation performed for a case of a plastic tube 0.04 m in diameter placed in the inner pipe resulted in a length requirement equal to 26.9 m. This represents a 24.5% reduction in length. The lengths recalculated with Eq. (26), (32) and (27), (33) were 26.87 m and 26.9 m, respectively. The rest of the results are presented in Table 2.

TABLE 2.
RESULTS FOR CASE STUDY WITH PLASTIC TUBE WITHIN THE INNER PIPE

Parameters	Cooling Water		Fluid Food (I)
	Outer Annulus (II_o)	Inner Tube (II_i)	
Mass Flow Rate (kg/hr)	5000	5000	2000
Equivalent Diameter $D_e(m)$ (Heat Transfer)	0.0927	0.060	0.0993 0.0670
Perimeter (m)	0.396	0.251	
Re (Heat Transfer)	19080	29470	4750 7040
Convective Heat Tr. Coeff. (W/m^2°C)	h_3 = 560	h_1 = 1240	h_1 = 300 h_2 = 270
Nu	117.70	165.60	49.30 67.50
Overall Heat Tr. Coeff. (W/m^2°C)	U_o = 181	U_i = 247	
Exit Temperatures (°C)	25.2	24.0	30.0
Log Mean Temperature Difference (°C)	30.7	31.1	
Heat Transfer Rates (W)	59,130	51,990	111,120

Comparing the results from Tables 1 and 2, it can be seen that the creation of an annular region within the inner pipe resulted in an even distribution of mass flow rates of cooling water between the inner and outer annuli. This increased the overall heat transfer coefficient on the outer annulus from 115 W/m^2°C to 181 W/m^2°C and the rate of heat transfer from 39, 230 W to 59,130 W.

Moreover, the exit temperature decreased 14.1 °C, from 39.3 °C to 25.2 °C, and the log mean temperature difference increased from 25.8 °C to 30.70 °C. On the other hand, the heat transfer rate through the wall of the inner pipe decreased from 71,890 W to 51,990 W, but the overall heat transfer coefficient decreased only by 9 W/m² °C and both the exit temperature and log mean temperature difference were slightly changed. The combination of all these changes resulted in a more efficient operation requiring a shorter heat exchanger.

CONCLUSIONS

The following conclusions can be drawn from the study:

(1) A mathematical model of a triple tube heat exchanger was derived. The analytical expressions can be used to predict bulk (cross-sectional area averaged) fluid temperatures at any axial location along the heat exchanger at each annulus and the central tube.

(2) A case study was presented with a complete computational procedure. The results obtained with the different equations were in excellent agreement and proved useful for heat exchanger design and evaluation purposes.

(3) The creation of an annular region in the inner pipe, by insertion of a plastic tube sealed at both ends, increases the overall heat transfer efficiency and reduces the length requirements of the heat exchanger.

LIST OF SYMBOLS

C =   Constant dependent upon pipe roughness (Eq. 36)
C_p =   Specific heat kJ/kg °C
D =   Diameter (m)
h =   Convective heat transfer coefficient (W/m² °C)
k =   Thermal conductivity (W/m °C)
L =   Heat exchanger length (m)
$\dot{M}$ =   Mass flow rate (kg/h)
Nu =   Nusselt number (hD_e/k)
P =   Perimeter (m)
P_r =   Prandtl number ($\mu C_p/k$)
q =   Heat flux (W)
Q =   Heat flux (W)
R_d =   Fouling factor (W/m² °C)
R_e =   Reynolds number ($\varrho V D_e/\mu$)

ϱ = Density (kg/m³)
T = Temperature (°C)
U = Overall heat transfer coefficient (W/m²°C)
V = Cross-sectional averaged fluid velocity
μ = Viscosity (Pa·s)
z = Axial position (m)

Subscripts

a = Relates to ambient
b = Relates to bulk conditions
I = Relates to fluid food flowing through middle annulus
IIi = Relates to cooling water flowing through inner pipe
IIo = Relates to cooling water flowing through outer annulus
i = Relates to inner surface of inner tube
o = Relates to outer surface of middle tube
(o) = Indicates temperatures at z = 0
(L) = Indicates temperatures at z = L
L = Relates to loss of heat to the surroundings and inner surface of outer tube
T = Relates to total heat transferred to or from the product
w = Relates to wall temperature conditions

Superscripts

I = Relates to fluid food
IIi = Relates to cooling water flowing through inner pipe
IIo = Relates to cooling water flowing through outer annulus

APPENDIX

Constants, A_{ij}, B_{ij}, C_{ij}, A_{4j}, B_{4j}, C_{4j} and D_{4j} and roots λ's used in Eq. (24)

$$A_{11} = a_{22}a_{33}/P_1$$

$$A_{12} = -a_{21}a_{33}/P_1$$

$$A_{13} = -a_{31}a_{22}/P_1$$

$$A_{21} = -(a_{12}a_{33}+a_{13}a_{22})/P_1$$

$$A_{22} = [a_{11}a_{33}+a_{13}(a_{21}-a_{31})]/P_1$$

$$A_{23} = [a_{11}a_{22}+a_{12}(a_{31}-a_{21})]/P_1$$

$$A_{41} = -a_{12}a_{33}/P_1$$

$$A_{42} = (a_{11}a_{33}-a_{13}a_{31})/P_1$$

$$A_{43} = a_{12}a_{31}/P_1$$

$$B_{11} = (\lambda_1-a_{22})(\lambda_1-a_{33})/P_2$$

$$B_{12} = a_{21}(\lambda_1-a_{33})/P_2$$

$$B_{13} = a_{31}(\lambda_1-a_{22})/P_2$$

$$B_{21} = [a_{12}(\lambda_1-a_{33})+a_{13}(\lambda_1-a_{22})]/P_2$$

$$B_{22} = [(\lambda_1-a_{11})(\lambda_1-a_{33})+a_{13}(a_{21}-a_{31})]/P_2$$

$$B_{23} = [(\lambda_1-a_{11})(\lambda_1-a_{22})+a_{12}(a_{31}-a_{21})]/P_2$$

$$B_{41} = a_{12}[(\lambda_1\lambda_2-a_{33}(\lambda_1+\lambda_2)]/P_4$$

$$B_{42} = -[\lambda_1\lambda_2(a_{11}+a_{33})-(a_{11}a_{33}-a_{13}a_{31})(\lambda_1+\lambda_2)]/P_4$$

$$B_{43} = a_{12}a_{31}(\lambda_1+\lambda_2)/P_4$$

$$C_{11} = (\lambda_2-a_{22})(\lambda_2-a_{33})/P_3$$

$$C_{12} = a_{21}(\lambda_2-a_{33})/P_3$$

$$C_{13} = a_{31}(\lambda_2-a_{22})/P_3$$

$$C_{21} = [a_{12}(\lambda_2-a_{33})+a_{13}(\lambda_2-a_{22})]/P_3$$

$$C_{22} = [(\lambda_2-a_{11})(\lambda_2-a_{33})+a_{13}(a_{21}-a_{31})]/P_3$$

$$C_{23} = [(\lambda_2-a_{11})(\lambda_2-a_{22})+a_{12}(a_{31}-a_{21})]/P_3$$

$$C_{41} = a_{12}(\lambda_1-a_{33})/P_5$$

$$C_{42} = [(\lambda_1-a_{11})(\lambda_1-a_{22})-a_{13}a_{31}]/P_5$$

$$C_{43} = a_{12}a_{31}/P_5$$

$$D_{41} = a_{12}(\lambda_2-a_{33})/P_6$$

$$D_{42} = [(\lambda_2-a_{11})(\lambda_2-a_{22})-a_{13}a_{31}]/P_6$$

$$D_{43} = a_{12}a_{31}/P_6$$

where

$P_1 = \lambda_1 \lambda_2$

$P_2 = \lambda_1(\lambda_1 - \lambda_2)$

$P_3 = \lambda_2(\lambda_2 - \lambda_1)$

$P_4 = (\lambda_1 \lambda_2)^2$

$P_5 = (\lambda_1)^2(\lambda_1 - \lambda_2)$

$P_6 = (\lambda_2)^2(\lambda_2 - \lambda_1)$

Values of the roots λ_1 and λ_2

$$\lambda_1 = [-b + (b^2 - 4ac)^{0.5}]/2a$$

$$\lambda_2 = [-b - (b^2 - 4ac)^{0.5}]/2a$$

where for parallel flow

$$a = 1$$

$$b = \beta_1 + \beta_2 + \beta_3 + \beta_4$$

$$c = \beta_1\beta_4 + \beta_2\beta_3 + \beta_3\beta_4$$

and for counter flow

$$a = 1$$

$$b = \beta_3 + \beta_4 - (\beta_1 + \beta_2)$$

$$c = \beta_3\beta_4 - \beta_1\beta_4 - \beta_2\beta_3$$

REFERENCES

JAKOB, M. 1949. *Heat transfer*, Vol. 1. John Wiley & Sons. New York.

HELDMAN, D.R. and SINGH, R.P. 1981. *Food Process Engineering*, 2nd Ed. Van Nostrand Reinhold/AVI, New York.

KAYS, W.M. and LONDON, A.L. 1964. *Compact Heat Exchangers*, McGraw-Hill, New York.

KERN, D.Q. 1950. *Process Heat Transfer*, McGraw-Hill, New York.

MARGITTAI, T.B. 1982. Fundamentally New Geometry for Heat Transfer Surface to Minimize or Even Completely Eliminate Fouling. Heat Transfer Magazine, August.

NAUGHTON, M. and SINGH, R.P. 1980. An Experimental Design for the Determination of Local Nusselt Numbers in an Annulus with Laminar, Pseudoplastic Flow. ASAE Tech. Paper No. 80-6014. American Society of Agricultural Engineers, St. Joseph, MI.

NORTH, R.S. and BACCHETTI, J.A. 1983. Cartridge Heat Exchangers Resist Fouling with Viscous Product. Chemical Processing, Mid-May.

PERRY, R.H. and CHILTON, C.H. 1973. *Chemical Engineer's Handbook,* 5th Ed. McGraw-Hill, New York.

SPALDING, D.B. and TABOREK, J. 1983. *Heat Exchanger Design Handbook.* Hemisphere Publ. New York.

STREETER, V.L. and WYLIE, E.B. 1979. *Fluid Mechanics*, 7th Ed. McGraw-Hill, New York.

WHITAKER, S. 1977. *Elementary Heat Transfer Analysis.* Pergamon Press, New York.

ROBOTIC HIGH PRESSURE WATER JET CUTTING
OF CHUCK SLICES[1]

W.K. HEILAND[2], R.P. KONSTANCE and J.C. CRAIG, JR.

U.S. Department of Agriculture, Eastern Regional Research Center
600 East Mermaid Lane
Philadelphia, PA 19118

ABSTRACT

With the objective of producing high quality and economical starting material for restructured beef products, the use of a high pressure water jet was investigated for excising objectionable material from slices of bone-in beef chuck. From the limited number of tests conducted, best conditions for a clean, smooth cut were obtained with a water jet orifice diameter of 0.15 mm (0.006 in), a water pressure of 380 MPa (55,000 PSI), a slice thickness of 19 mm (3/4 in) and a linear cutting speed of 10.9 m/min (430 in/min). A preliminary cost comparison indicated that a fully automated line had a greate economic advantage over the manual method.

INTRODUCTION

Water erosion is a well known natural phenomenon, responsible for the smoothing of old mountain ranges, or the gouging of valleys as awesome as Arizona's Grand Canyon. Using the water jet, man has harnessed this phenomenon to cut materials as soft and flimsy as disposable baby diapers or as hard as rock, even man-made ceramics. The water jet may be used in combination with mechanical cutters or the jet may be pulsed. Both are effective assists in fracturing brittle materials and are applied in mining and oil well drilling (Saunders 1977; Lee 1975; Maurer 1975). The addition of long chain polymers to the water reduces the diversion of the jet stream (Franz 1972), while the addition of abrasives by means of a secondary jet allows for the cutting of very hard and tough materials, like ceramics (Smoluk 1986). The dustless action of the

---

[1]Reference to brand or firm name does not constitute endorsement by the U.S. Department of Agriculture over others of a similar nature not mentioned.

[2]Correspondence address and to whom reprint requests should be directed: W.K. Heiland, U.S. Department of Agriculture, 600 East Mermaid Lane, Eastern Regional Research Center, Philadelphia, PA 19118.

water jet makes it environmentally safe for cutting asbestos sheets and brake linings (Martin 1980).

Commercial applications of water jet technology in the food area are few. Brierly (1975) reported the halving of freestone peaches and Shield *et al.* (1973) investigated high speed cutting of lettuce stems. The water jet is ideally suited for robotic positioning due to its omnidirectional feature and instantaneous on/off capability. An automatic and continuous process envisioned for the preparation of restructuring material (Heiland *et al.* 1987) would utilize high pressure water jets for a sanitary, high speed excision of objectionable material (bone, fat, gristle) from slices of beef chuck. The two key elements of this automatic process are the detection by an optical sensor (Konstance *et al.* 1988) and the excision of objectionable materials. The objective of this study was to demonstrate the potential of water jets for this excision operation.

MATERIALS AND METHODS

USDA choice grade, square-cut chucks (#113, NAMP, 1984), Yield Grade 2 steers were used in this study. The chucks were frozen at $-20\,°C$, then tempered at $-5\,°C$ for two days and sliced on a band saw. The saw (Biro Manufacturing Co., Marblehead, OH, Model #33) had a custom made saw table extension to accomodate chucks weighing up to 53 kg and a base extension to prevent the saw from tipping. The chucks were sliced, starting from the fifth rib, to different thicknesses of 12.5, 25, 50 and 100 mm. These slices were vacuum packaged (Smith Equipment Co., Clifton, NJ, Supervac Model GK 120) and returned to $-20\,°C$ storage.

A Water Jet Knife, (Flow Systems, Inc., Kent, WA) that consisted of small sapphire nozzles and a model 11XD-MK2-55 internsifier pump capable of delivering 4.69 L/min (1.24 Gpm) at 380 MPa (55,000 PSI) was used. At this pressure, water is 12% compressed (Martin 1980) and the water jet operates with a stream velocity of Mach 3 (Buck *et al.* 1979). Remote manipulation of the nozzles was accomplished with a 59 kg (130 lb) industrial programmable robot (ASEA Robotics, Inc., New Berlin, WI). This combined system was located in the Mechanical Engineering Department, College of Engineering, University of Rhode Island. Experiments were conducted at URI to determine the maximum linear traverse speed for each condition that cut completely through red meat, fat and connective tissue. The following variables were studied: (1) meat temperature (frozen versus unfrozen), (2) slice thickness, (3) intensifier pump pressure, (4) nozzle orifice diameter of the water jet and (5) speed limitations imposed by the robot's inertia when programmed to follow intricate patterns, e.g., those required for the excision of bone.

Residual bone matter was determined by measuring calcium concentration using atomic absorption (AOAC 1984).

TABLE 1.
MAXIMUM LINEAR TRAVERSE SPEEDS OF WATER JET THAT RESULTED
IN COMPLETE SEVERING OF RED MEAT, FAT AND CONNECTIVE TISSUE
IN UNFROZEN (+3 °C) SLICES OF BEEF CHUCK - WATER JET OPERATED
WITH 380 MPa PRESSURE AND A 0.15 mm NOZZLE ORIFICE DIAMETER

Slice Thickness (mm)	Linear Traverse Speed (m/min)	Kerf Loss[1]		Remarks
12.5	25	very little	(< 2%)	clean cut through full thickness
25	5	very little	(< 2%)	clean cut through full thickness
50	1	great	(> 5%)	lower half of cut very rough and wide
100	0.2	excessive	(> 10%)	lower half of cut extremely ragged and very wide

[1]Based on an average length of excision cut of 2.5 m/slice and an average slice area of 0.1 m².

RESULTS AND DISCUSSION

The linear traverse speeds that resulted in complete cuts through beef chuck slices of varying thickness are shown in Table 1. Red meat, fat and connective tissue were completely severed while bone was only slightly scored. All data in Table 1 were obtained with the intensifier pump operating at 380 MPa and a 0.15 mm nozzle orifice diameter. Based on a number of preselected linear traverse speeds Table 1 indicates that the linear traverse speeds V are inversely proportional to the 2.32 power of the slice thickness t:

$$\frac{V_1}{V_2} = (\frac{t_2}{t_1})^{2.32} \tag{1}$$

For a water pressure of 380 MPa and a 0.2 mm orifice the exponent of this relationship was found to be 1.82. Because of the preselected linear traverse speeds and the somewhat subjective observation of the quality of the cut the linear traverse speeds are assumed to be inversely proportional to the square of the slice thickness, and Eq. (1) becomes;

$$\frac{V_1}{V_2} = (\frac{t_2}{t_1})^2 \tag{2}$$

While larger orifice diameters allowed faster traverse speeds (e.g., by using a 0.2 mm orifice, a 25 mm thick slice could be cut at 7.5 m/min and a 100 mm slice could be cut at 0.6 m/min with a 0.25 mm orifice), more water was required which reduced the number of water jets that can be operated from one intensifier pump (the intensifier pump used had the capacity to simultaneously operate six nozzels with a 0.15 mm diameter or one nozzel which a 0.33 mm diameter orifice). Without additives and at pressures up to 380 MPa, slices 50 mm thick or thicker could not be cut cleanly, regardless of orifice diameter. Also, kerf losses increased with orifice diameter.

An attempt was made to establish conditions under which the water jet would deflect when impacting bone. It was the objective to produce an excision that followed the surface contour of a bone, especially when not perpendicular to the slice surface. Impingement of the jet on bone resulted in reflection in all cases at any angle of impingement, even at lower intensifier pump pressures (e.g., 275 MPa). The impingements caused a slight scoring of the bone surface; score depth was visually judged to be inversely proportional to the linear traverse speed of the water knife. This erosive action removed a small amount of bone in powdered form but never generated any bone chips, a very desirable, inherent feature of water jet excision.

Cutting of slices of frozen ($-5\,°C$) beef chuck could be done at linear traverse speeds equal to those of unfrozen ($+3\,°C$) slices of equal thickness. After cutting, refreezing along the cut lines did not occur.

Meat samples, immediately adjacent to bone, that were subjected to water jet impingement, were analyzed to determine evidence of residual, powdered bone matter (mg/g calcium). The results, shown in Table 2, indicate that the calcium concentration of these samples, including the control samples from the same slices, is well within the range of naturally occurring calcium (0.09 – 0.13 mg/g)(Watt et al. 1963). Bone powder, that may be created, is evidently washed away by the very stream that produces it.

Removal of objectionable tissue and bone required that the water jet was guided through intricate paths and patterns. Inertia limitations of the robot arm that controlled the water jet lowered the high linear speeds otherwise possible with 12.5 mm thick slices. At a linear speed of 10.9 m/min, precise control of the robotic arm through intricate paths was "state of the art" and Eq. (2) yielded a corresponding slice thickness of 19 mm. At this slice thickness, anatomical changes between slices are manageable during the automatic excision of objectionable material.

This study demonstrated the applicability of robotic water jet excision of objectionable material from slices of beef chuck. Data from this study were used in a cost study comparing manual versus automated preparation of starting material for restructured beef products. This cost study showed that the automated system with an annual production rate of 7.6 million kg (16.8 million lb) would save at

TABLE 2.
CALCIUM CONCENTRATION IN MEAT SAMPLES
CUT BY WATER JET ADJACENT TO BONE

Sample #	Sample Weight (g)	Calcium Concentration (mg/g)
1	7.16	0.139
2	3.86	0.109
3	2.18	0.138
4	2.59	0.100
5	4.05	0.084
Control	4.29[1]	0.160[2]

[1]Average sample weight over 6 samples.
[2]Average calcium concentration of control samples.

least $0.5 million over a manual method employing 20 meat cutters each in two shifts. Utilizing a slice thickness of 19 mm and a 0.15 mm nozzle orifice diameter, the automated system made optimum use of the intensifier pump's capacity. At the same time the linear traverse speed did not exceed the inertia limitations of the robot, the number of slices per chuck was manageable and the anatomical changes between subsequent chuck slices was minimal.

ACKNOWLEDGMENTS

REFERENCES

AOAC. 1984. *Methods of Analysis*, 14th ed. Assoc. Official Analytical Chemists, Washington, DC.

BRIERLEY, W.H. 1975. Applications of water jet cutting. Proceedings of the Workshop on the Application of High Pressure Water Jet Cutting Technology. University of Missouri. Nov. 10–11.

BUCK, E.J. and ZUELOW, D.L. 1979. New techniques in water jet cutting. Society of Manufacturing Engineers. Technical paper MR 79-576.

FRANZ, N.C. 1972. Fluid additives for improving high velocity jet cutting. First International Symposium on Jet Cutting Technology, University of British Columbia, Canada, BHRA Fluid Engineering, Cranfield, April, p. A7-93.

HEILAND, W.K., KONSTANCE, R.P. and CRAIG, J.C., JR. 1988. Automatic production of starting material for restructured beef. Patent Pending.

KONSTANCE, R.P., HEILAND, W.K. and CRAIG, J.C., JR. 1988. Component recognition in beef chuck using colorimetric determinations. J. Food Sci. 53(3), 971.

LEE, R.D. 1975. The application of high pressure water jets to cutting. Mecanique, Aug.-Sept., p. 23.

MARTIN, J.M. 1980. Using water as a cutting tool. American Machinist. April. p. 123.

MAURER, W.C. 1975. Increased speed and greater economy of oil well drilling when combining drill bits with high pressure jets. Proceedings of the Workshop on the Application of High Pressure Water Jet Cutting Technology. Univeristy of Missouri. Nov. 10-11.

NAMP. 1984. *Meat Buyer's Guide,* National Assoc. of Meat Purveyors. McClean, VA.

SAUNDERS, D.H. 1977. Water as a cutting tool. Engineering. April, p. 297.

SCHIELD, M. and HARRIOTT, B.L. 1973. Cutting lettuce stems with a water jet. Trans. ASAE. p. 440.

SMOLUK, G.R. 1986. Water jet cutting goes robotic. Modern Plastics. Sept. p. 54.

WATT, B.K. and MERRIL, A.L. 1963. Composition of Foods. Agricultural Handbook #8. U.S. Department of Agriculture, Washington, DC. U.S. Government Printing Office.

A STUDY OF DRAG FORCES ON SOLID SPHERICAL PARTICLES IN POWER LAW BOUNDED FLOW: APPLICATIONS TO ASEPTIC PROCESSING[1]

GIRISH SUBRAMANIAM
Graduate Assistant

and

CARLOS A. ZURITZ[2]
Assistant Professor

Department of Agricultural Engineering
The Pennsylvania State University
University Park, PA 16802

ABSTRACT

Drag forces on rigid spherical particles suspended at specific points in a tube carrying viscous solutions of sodium carboxymethylcellulose (CMC) were measured using a load cell. Polystyrene spheres of diameter 1, 2.22 and 3.175 cm were used in a plexiglass tube of 4.75 cm internal diameter. The range of consistency coefficient of the carrier fluid studied was 5 to16 Pa-s^n. Mass flow rate was varied between 0.01 and 0.9 kg/s. The drag coefficient-generalized particle Reynolds number correlation developed from linear regression was: $Cd = 101.35/[(N_{Re})p]^{0.84/n}$. This correlation may be used to estimate drag forces on suspended spherical food solids in aseptic holding tubes.

INTRODUCTION

Accurate information about particle-fluid dynamics in aseptic holding tubes is required for safe and efficient process control and sterilization with minimum overprocessing. A good design of the aseptic holding tube is as important as that of the heat exchanger.

The motion of suspended soild particles in flowing liquids has been and still is of interest in many areas of engineering. Although there exists considerable literature on the subject of such two-phase flows, very little research effort has

been oriented towards dynamic forces on large particles suspended in non-Newtonian liquids flowing in bounded regions such as pipes, a feature of aseptic process systems.

Knowledge of the force balance on a body is a prerequisite to describing its motion. A predominant force governing the solid particle motion in viscous flow is the **drag force**, which is responsible for pulling the solid along with the liquid. The existence of a velocity profile in the carrier fluid itself makes the prediction of suspended particle motion difficult because, depending on the radial location of the body, the drag on it is significantly different. Moreover, radial migration would lead to constantly changing drag effects.

Theoretical prediction of drag forces involves piecewise integration of localized pressure and viscosity effects over the entire surface of the submerged body, which is a full scale numerical analysis. Similarly, experimental measurement of the drag force on a particle moving with the carrier liquid inside a holding tube poses many practicle difficulties. In the present study, the problem has been simplified to the analysis of drag effects on rigid spheres fixed at specific radial locations under power law or the Ostwald-de Waele flow in a holding tube, as a first attempt to better understand two-phase flows in the light of aseptic processing of particulate foods.

Saffman (1965 and 1968) derived a mathematical equation for the nonrotational lift force due to shear flow on a suspended sphere. Extensive experimentation on radial movement of small, neutrally bouyant spheres in viscous flow has been done by Segre and Silberberg (1961). Goldsmith and Mason (1961) found that rigid particles migrated to intermediate radial positions, while deformable bodies migrated to the flow-axis. An interesting result was obtained by Rubinow and Keller (1961) for the lift force on a sphere rotating in a fluid (Magnus lift). The leading term in this expression is independent of fluid viscosity and is similar to the lift formula for two-dimensional potential flow about an airfoil.

Tritton (1959) described measurements of the drag force on circular cylinders, made by observing the bending of quartz fibres in a stream, and applying simple bending moment theory to calculate the force exerted on the fibre. He related drag coefficient to Reynolds number in the range of 0.5 to 100 and compared his results with other experimental measurements on drag.

Happel and Byrne (1954) derived mathematical expressions for the viscous force exerted on a sphere moving along the axis of a cylinder and the fluid pressure drop. A simple relationship was also obtained for pressure drop through a dilute system of assemblages of spherical particles. Odar and Hamilton (1963) proposed a detailed equation for the force exerted on a sphere accelerating in a still fluid, which was reduced to the known theoretical solution for the case of low velocity and large acceleration.

Owing to the nonlinearity and interdependence of the governing equations, numerical solutions have been sought by some in the broad area of two-phase

flow. Sastry and Zuritz (1987) wrote a code in BASIC to track a spherical particle moving within an aseptic holding tube along with a non-Newtonian (power law) liquid, under the influence of the drag force, Saffman and Magnus lift forces and buoyancy effects. Sastry and Zuritz used empirical equations to calculate the above mentioned forces.

Tomita (1959) analyzed the motion of pseudoplastic and dilitant fluids past a sphere using equations of minimum dissipation of energy. Non-Newtonian flow past a sphere has been the focus of Slattery (1960), Ziegenhagen (1961) and Caswell and Schwartz (1962) as well. A boundary-layer analysis of two-dimensional and axi-symmetric flow of fluids described by the Ostwald-de Waele model around obstacles was carried out by Bizzell and Slattery (1962). They presented a relationship between the flow behavior index (n) and the point of separation of flow on the particle surface.

Mhatre and Kintner (1959) measured terminal velocities of liquid drops in solutions of sodium carboxymethylcellulose (CMC), a liquid of non-Newtonian properties, and concluded that the apparent viscosity of the solution is the key to prediction of terminal velocities of liquid drops moving through pseudoplastic liquids. Drag coefficients for spheres moving through CMC solutions were measured by Slattery and Bird (1961) with the assumption that the behavior of CMC solutions could be better approximated by the Ellis model, than by the Ostwald-de Waele representation. Terminal velocities of spheres falling in a large body of the quiescent CMC solution were measured and a dimensionless friction factor or the drag coefficient was calculated using an arbitrary definition. Correlations for the drag coefficient in terms of the generalized Reynolds number were presented.

Wasserman and Slattery (1964) calculated upper and lower bounds to the drag coefficient for a sphere moving through a power law fluid using variational methods. The authors compared the mean value of the drag coefficient with the experimental data of Slattery and Bird (1961), and concluded that, simple rheological models may not completely describe the behavior of fluids like CMC solutions, and that additional experimental data are necessary to clarify the situation.

The drag coefficient-generalized Reynolds number approach is quite useful in expressing dependent variables in a problem in terms of independent variables and system parameters. Although, such relationships have been established for drag phenomena in unbounded or large bodies of static fluids, more attention needs to be paid to the case of solid spheres suspended in non-Newtonian flow in bounded regions such as tubes of dimensions of the same order of magnitude as that of the spheres. The objectives of the present study were to measure the drag force on single spheres in a holding tube carrying a non-Newtonian liquid for various sphere sizes, radial positions, fluid viscosities and mass flow rates, and to develop a correlation between drag coefficient and Reynolds number.

THEORETICAL CONSIDERATIONS

A dimensionless form of the stress equations of motion for a power-law or Ostwald-de Waele fluid is presented below.

$$\underline{U} \cdot \nabla^* \underline{U} \;=\; - \nabla^* P/2 + [1/(N_{Re})_{gen}] \, \nabla^* \cdot (K_0 \underline{D}) \tag{1}$$

where;

$$\nabla^* \;=\; D_c \, \nabla \tag{2}$$

$$\underline{U} \;=\; \underline{v}/v_c \tag{3}$$

$$P \;=\; 2p/(\rho v_c^2) \tag{4}$$

$$(N_{Re})_{gen} \;=\; (\rho \, v_c^{2-n} \, D_c^n)/m \tag{5}$$

$$K_0 \;=\; |\sqrt{[(\underline{D}:\underline{D})/2]}|^{(n-1)} \tag{6}$$

$$\underline{D} \;=\; (\nabla^* \underline{U} + \nabla^* \underline{U}^T)/2 \tag{7}$$

Thus, the basic variables in Eq. 4 are the velocity $\underline{U}$, pressure P, the spatial coordinates X_1, X_2 and X_3, the flow behavior index n and the generalized Reynolds number $(N_{Re})_{gen}$, all dimensionless quantities. The velocity is a function of pressure, spatial position, flow behavior index and Reynolds number. This dependency can be expressed as:

$$\underline{U} = \underline{U} \, (P, X_1, X_2, X_3, n, (N_{Re})_{gen}, N_{BC}) \tag{8}$$

A similar functional relationship can be written for the pressure, as follows.

$$P = P \, (\underline{U}, X_1, X_2, X_3, n, (N_{Re})_{gen}, N_{BC}) \tag{9}$$

where, N_{BC} is a dimensionless group representing all new parameters appearing in the boundary conditions.

The drag force (F_d) experienced by a particle in tube flow is the axial component of the force exerted by the fluid on the particle. This force is the net resultant of the pressure effects and the shear stresses due to velocity gradients at the particle surface, and is obtained as a surface-averaged force, by piecewise integration of a differential force dF, over the entire surface of the sphere. Thus, the drag force (F_d) on the sphere, represented by a particle drag coefficient (C_d) is a spatially integrated force, and therefore independent of the spatial coordinates. Then the followng functional relationship can be obtained.

$$C_d = C_d (n, (N_{Re})_{gen}, N_{BC}) \tag{10}$$

For the case of a spherical particle suspended in tube flow, the only boundary parameters introduced are the particle diameter (D_p) and particle velocity (V_p), at the surface of the sphere, and the tube radius (R), at the tube wall. For a given sphere at a particular position in the tube, the characteristic velocity in the Reynolds number formulation (Eq. 5) can be taken as the particle-to-fluid relative velocity (V_{pf}), defined as the difference between the fluid streamline velocity "through" the particle center $V_{f(r)}$ and the particle axial velocity.

For laminar flow, the use of $(V_{f(r)})$ in the characteristic velocity definition accounts for the radial position of the particle and the tube size. Then, by defining the characteristic length in Eq. 5 to be D_p, the Reynolds number thus obtained is the generalized particle Reynolds number $(N_{Re})_p$ for non-Newtonian flow over submerged bodies. For the special case of a fixed particle, the relative velocity (V_{pf}) is equal to $V_{f(r)}$. If further, and as a first approximation, additional parameters arising from N_{BC} are ignored, Eq. 10 for the particle drag coefficient reduces to the following form.

$$C_d = C_d (n, (N_{Re})_p) \tag{11}$$

where;

$$(N_{Re})_p \;\; = \;\; (\rho \, V_{f(r)}^{2-n} \, D_p^n)/m \tag{12}$$

It is evident from the above equation that the drag coefficient (C_d) for the particle is a function of the flow behavior index (n) and the generalized particle Reynolds number $((N_{Re})_p)$. Therefore, the drag force on the sphere is also dependent on the same two parameters.

Slattery and Bird (1961) have presented an explicit relationship between the drag coefficient and the Reynolds number for Ellis model fluids (Skelland 1967) as:

$$C_d \;\; = \;\; 24/(N_{Re})_{p,E} \tag{13}$$

The above correlation may be transformed for power law fluids as presented below.

$$C_d \;\; = \;\; 24/[(N_{Re})_p]^{1/n} \tag{14}$$

When n equals 1, the above equation reduces to Stokes law for drag on a sphere. Equation 14 is applicable only to unbounded creeping flow. However, the above correlation does suggest that, for the present case of a sphere in a tube also, C_d

might vary as the reciprocal of the nth root of $(N_{Re})_p$, as expressed below.

$$c_d \quad \sim \quad 1/[((N_{Re})_p)]^{1/n} \tag{15}$$

The above relation might indicate that an explicit form of this functionality could be determined from an experimental study of the particle drag coefficient (C_d) with respect to the generalized particle Reynolds number ($(N_{Re})_p$).

MATERIALS AND METHODS

In order to carry out drag force measurements for the situation under study, different test spheres were suspended at specific locations within a pipe of circular cross-section (4.75 cm in diameter), and a viscous non-Newtonian liquid was circulated in a closed loop, as shown in Fig. 1. The force was measured directly using a load cell (LCL 227G; Omega Engineering) calibrated by recording the strain indicated for various known weights between 10 and 100 g.
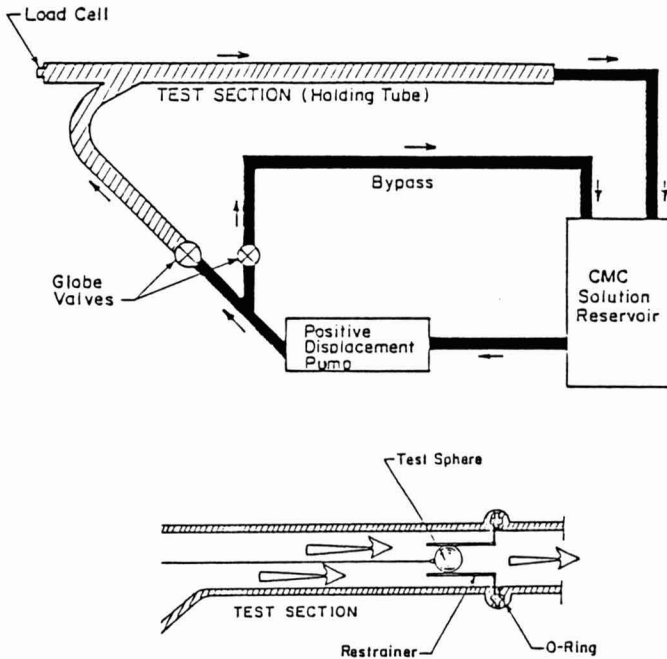

FIG. 1. SCHEMATIC OF THE FLOW SYSTEM

Three polystyrene spheres sized 1 cm, 2.22 cm and 3.175 cm in diameter, were tested. The spheres were nearly neutrally buoyant in the carrier fluid with specific gravity values of 1.031, 1.004 and 1.051, respectively. The non-Newtonian fluids used were aqueous solutions of sodium carboxy-methylcellulose or CMC (TIC Gums Inc.) of viscosities or consistencies between 5 and 16 Pa-s^n. Solution densities varied from 1.001 to 1.009 g/mL. The Ostwald-de Waele model was assumed to represent the rheology of the soltuions. Consistency coefficients (m) and flow behavior indices (n) were determined from apparent viscosity (μ_{app}) and rate of shear ($\dot{\gamma}$) measurements (made using a Brookfield digital viscometer, model RVTD with spindle LV #2 and in a 600 mL beaker) by linear regression analysis according to the following definitions.

$$\mu_{app} = m \dot{\gamma}^{(n-1)} \tag{16}$$

$$\log(\mu_{app}) = \log(m) + (n-1)\log(\dot{\gamma}) \tag{17}$$

The spheres were connected to the load cell by a thin wire (0.1 mm in diameter). The drag on the wire was accounted for in determining the net drag force on the spheres. The wire was long enough to position the spheres downstream beyond entrance effects in the region of fully developed flow. The entrance length was estimated using Eq. 18 (Whitaker 1968).

$$L_e = 0.035 D (N_{Re})_t \tag{18}$$

where;

$$(N_{Re})_t = [\rho V_{av}^{(2-n)} D^n]/[2^{(n-3)} m((3n+1)/n)^n] \tag{19}$$

In order to study the effect of radial location of the particles within the tubes, each sphere was restricted from lateral movement with the help of a set of thin steel limbs (referred to as a restrainer) bent in the direction of flow, forming a small fence around the particle. These limbs were welded to a steel gasket that slipped into position with an O-ring between the pipe-flanges in the test section (Fig. 1). One restrainer was fabricated for each test sphere and could be easily affixed to and removed from the system as required. It was ensured that there was some play between the limbs and the ball to avoid lateral pressure on the spheres and that the connecting wire was at full-stretch during the experiments. Since the restrainers were constructed from thin steel wire (0.8 mm diameter), their effect on the flow profile was neglected.

Drag force readings on the test spheres were taken for various values of mass flow rate, fluid consistency and the two radial positions. Table 1 lists the different parameters studied in these experiments.

TABLE 1.
RANGE OF PARAMETERS STUDIED

1.	Particle size:	Sphere diamters (cm) 3.175 2.22 1.00
2.	Particle radial location:	Axis & near the wall
3.	Fluid viscosity:	m-value (Pa-s^n) 13 – 16 (High) 8.5 – 10 (Medium) 5 – 6.5 (Low)
4.	Mass flow rates:	(kg/s) 0.01 – 0.9
5.	Reynolds numbers:	0.001 – 0.5

Appreciating that the relative motion between the solid and fluid phases plays a key role in the heat transfer from the carrier liquid to the suspended food particle, the tests on the fixed spheres were conducted at reduced flow rates. This was an attempt to match the magnitude of the particle Reynolds numbers $((N_{Re})_p)$ with values encountered in the case of free-flowing particles in industrial scale aseptic processing operations. Therefore, the range of flow rates tested (between 0.01 and 0.9 kg/s) included values considerably lower than the typical 0.5 to 1 kg/s levels used in the industry.

First, a very viscous solution of CMC was prepared by hand-mixing CMC powder with water such that, the consistency coefficient (m) of the resulting solution was well above 15 Pa-s^n (the highest viscosity level to be tested). The entire quantity was then poured into a reservoir connected to the system of holding tubes via a variable speed positive displacement pump (Waukesha sanitary pump, size 130), as shown schematically in Fig. 1. The CMC solution was then recirculated through the bypass alone, while its viscosity was tested about five times until the initial effects of agitation and shear deformation due to pumping had subsided. Thereafter, the solution was carefully diluted with water until a consistency coefficient of about 15 Pa-s^n was attained so that it would be in the high viscosity range, which was arbitrarily decided as comprising of m-values greater than 13 Pa-s^n. The density of this solution was then measured using a 100 mL graduated cylinder and a Mettler PE 360 balance.

After ensuring that all connections were properly made, the control valve in the test section was opened and the CMC solution allowed to flow in the tube

housing the sphere connected to the load cell. The pump and valve settings were adjusted to obtain the desired mass flow rates in the test section which were measured by the bucket-and-stop-watch method.

Having completed one test for a given sphere and position, all flow of the CMC solution was diverted through the bypass for recirculation, while another sphere was installed for testing. The viscosity of the CMC solution was measured at the beginning and the end of each test and the average value of "m" was taken to represent the viscosity of the CMC solution during that test.

In order to calculate the drag force on the spheres alone, the drag on the wire, by itself, was measured by running the above test on the wire alone, without any sphere attached to it. The viscosity of the CMC solution during this series of tests was also recorded.

After the spheres and the wire were tested at high viscosity, the CMC solution was diluted again, down to consistency of about 10 Pa-s^n to be in the medium viscosity range (8.5 to 10 Pa-s^n) and data acquisition carried out for the three test spheres and also the wire at each step. Finally, the low viscosity range of m-values between 5 and 6.5 Pa-s^n was investigated in the same manner.

A second set of data was collected for the same parameters listed in Table 1, using a thin cotton-polyester string of diameter 0.13 mm in place of the metal wire.

RESULTS AND DISCUSSION

Since the load cell registered the total axial pull of the carrier liquid on the sphere and the material connecting it to the load cell, the measured drag force (F_t) is the sum of the drag on the sphere and that on the connecting wire or string. Therefore, in order to obtain the value of the drag force on the sphere alone, the contribution of the wire/string was subtracted from the total drag. The effects of gravity or lift on the spheres and the wire were not measured by the load cell as it was calibrated for axial loads only. Discussed in detail below, are the results of the tests conducted using the wire.

Wire-and-Sphere Experiments

During the experiments, the CMC solution was being recirculated constantly in the holding tube system by means of the pump, which caused a gradual mechanical breakdown of the liquid. Therefore, considering that the viscosity of the carrier liquid, specified by the constants "m" and "n" of the power law model for non-Newtonian liquids, was slightly different at the time of drag measurements on the wire from that at the time of testing with the spheres, a generalized approach using **dimensionless** representative quantities was adopted.

A drag coefficient for the wire was defined as follows.

$$C_{dw} = 2F_w / (\rho A V_{av}^2) \tag{20}$$

The generalized tube Reynolds number for laminar flow of a non-Newtonian liquid in a tube was calculated for each flow condition using Eq. 19. $Log[C_{dw}]$ values were regressed against $log[(N_{Re})_t]$ values with a linear equation (Fig. 2, $r^2 = 0.98$). The drag force on the wire for every tube Reynolds number, defined by the experimental parameters and variables, was calculated from the regression line using Eq. 20. The net drag force on the sphere (F_d) for the corresponding tube Reynolds number, was obtained by subtracting F_w from F_t.

The behavior of drag force on the sphere against mass flow rate as a function of particle diameter and fluid viscosity was then studied and is discussed below.
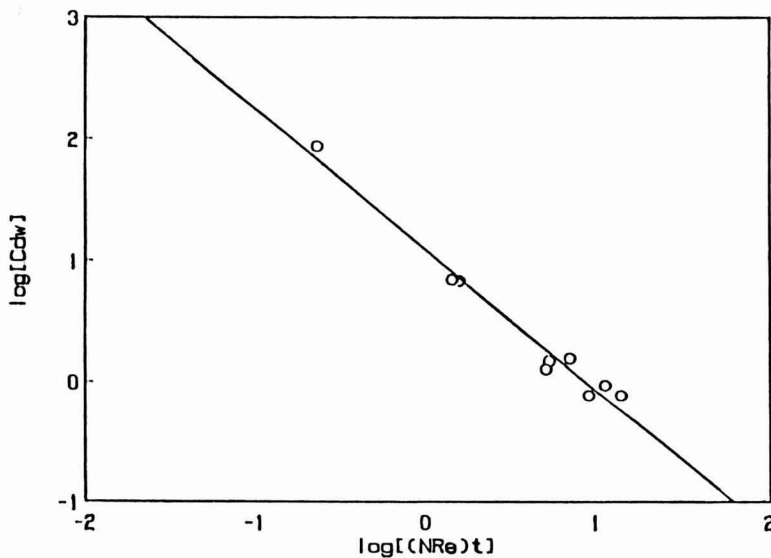

FIG. 2. LOGARITHMIC PLOT OF WIRE DRAG COEFFICIENT
VERSUS TUBE REYNOLDS NUMBER

Particles Located Along the Tube Axis

Representative results of F_d versus M_f plots as a function of particle size are shown in Fig. 3 for the medium viscosity range. It can be observed that the magnitude of the drag force on the large sphere changes rapidly at low flow rates, while that on the small sphere seems to have attained a constant value in that flow range. As expected, the drag force experienced by the spheres decreased with decreasing viscosity.
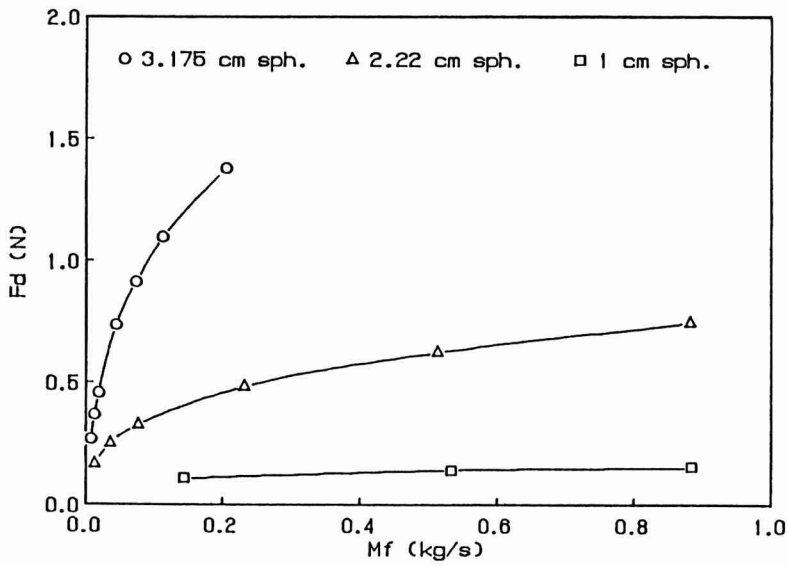
FIG. 3. NET DRAG FORCE VERSUS MASS FLOW RATE FOR
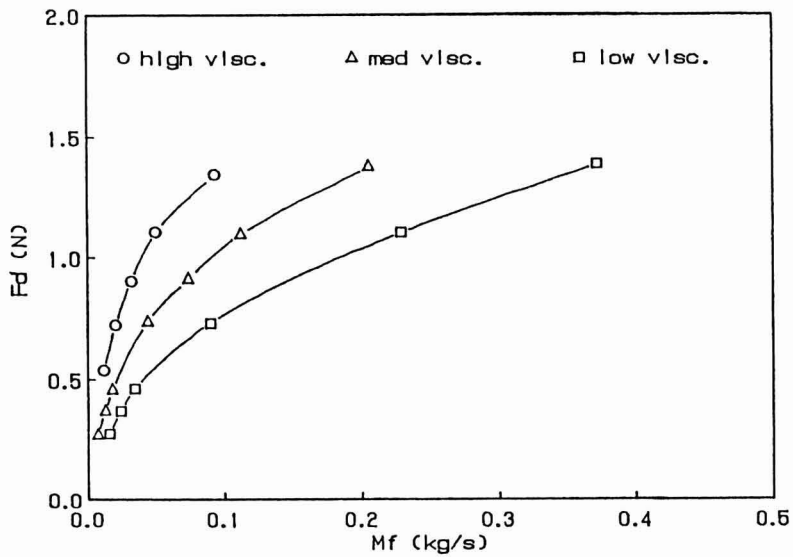SPHERES AT THE AXIS AT MEDIUM VISCOSITY

FIG. 4. NET DRAG FORCE VERSUS MASS FLOW RATE FOR
THE LARGE SPHERE AT THE AXIS

Plots of drag force versus mass flow rate as a function of fluid viscosity for the large, medium and small test spheres are presented in Fig. 4, 5 and 6, respectively. The curves tend to merge towards the origin which is in keeping with the fact that there is no drag without flow. In Fig. 5 for the medium test sphere, the medium viscosity line overlaps the high viscosity line implying that at certain flow rates the drag force on the sphere was greater in the medium viscosity solution than in the high viscosity. Figure 6 for the small sphere shows this effect very prominently as the high viscosity line is below the medium and low viscosity lines. These contradictory results are due to errors generated by the use of one regression line in Fig. 2 to represent the drag coefficient of the wire, whereas some degree of scatter is visible in that graph. Subsequent exponentiation to obtain the drag force on the wire further magnified such deviations. A deviation of 0.1 in a $\log[C_{dw}]$ value of 1 would reflect as an error of up to 26% in the value of F_w, and subsequently in F_d. The major factor contributing to the behavior shown in Fig. 6 could be that the drag force on the wire was considerably greater than on the small test sphere in the high viscosity range, and consequently, errors introduced by the wire-correction are relatively greater in this case. This effect can be better appreciated by comparing Fig. 4, 5 and 6 with Fig. 7, 8 and 9 which represent the total drag force before the deduction of the drag force on the wire.
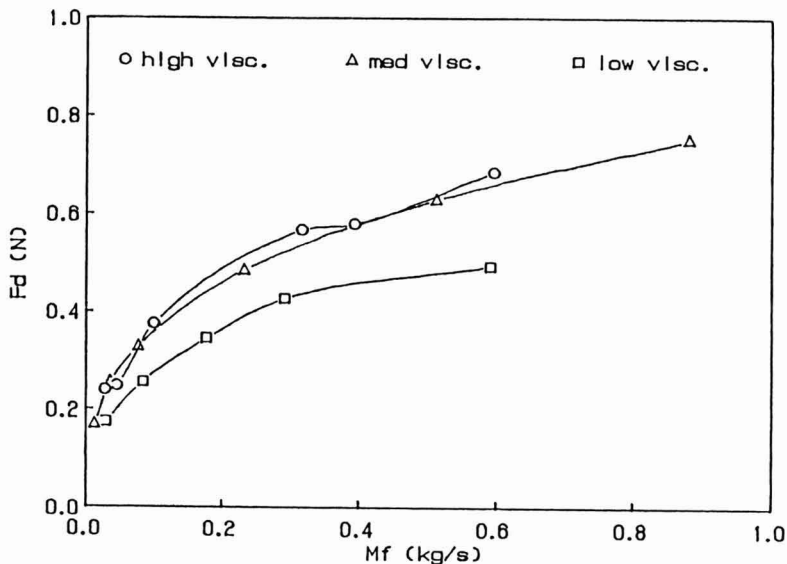

FIG. 5. NET DRAG FORCE VERSUS MASS FLOW RATE FOR
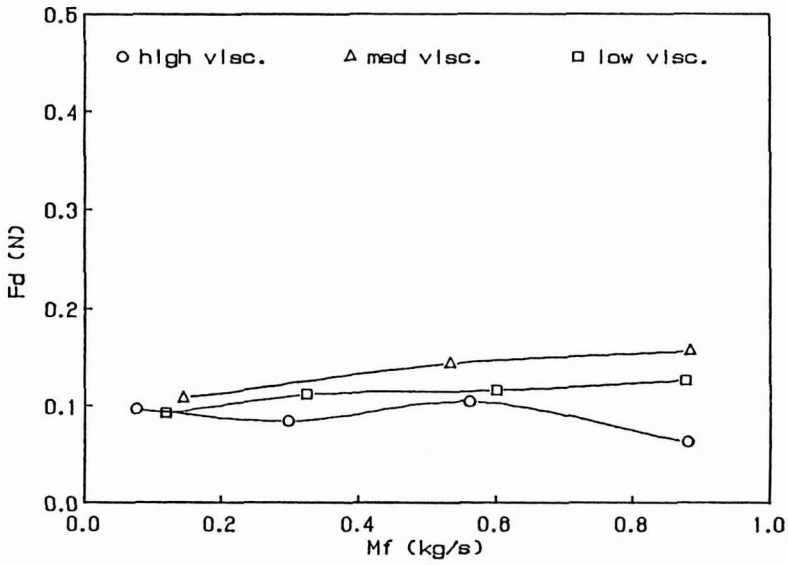THE MEDIUM SPHERE AT THE AXIS

FIG. 6. NET DRAG FORCE VERSUS MASS FLOW RATE FOR
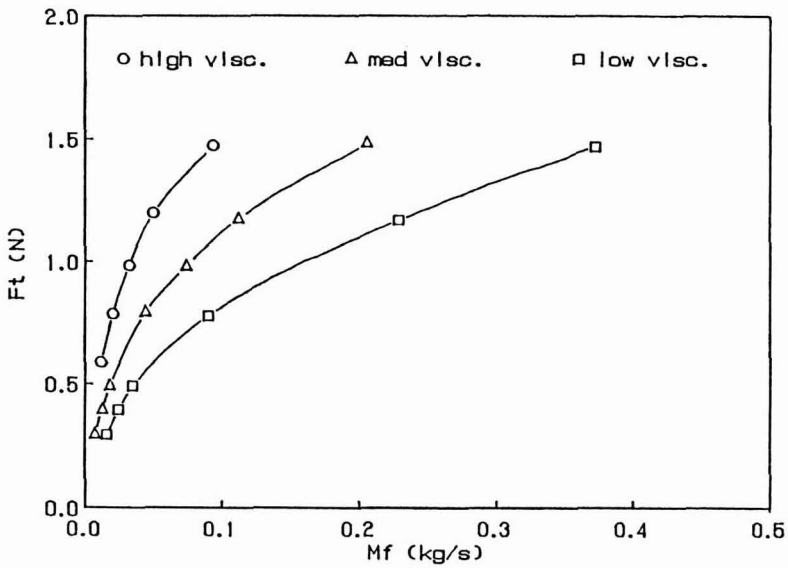THE SMALL SPHERE AT THE AXIS

FIG. 7. TOTAL DRAG FORCE VERSUS MASS FLOW RATE FOR
THE LARGE SPHERE LOCATED AT THE AXIS
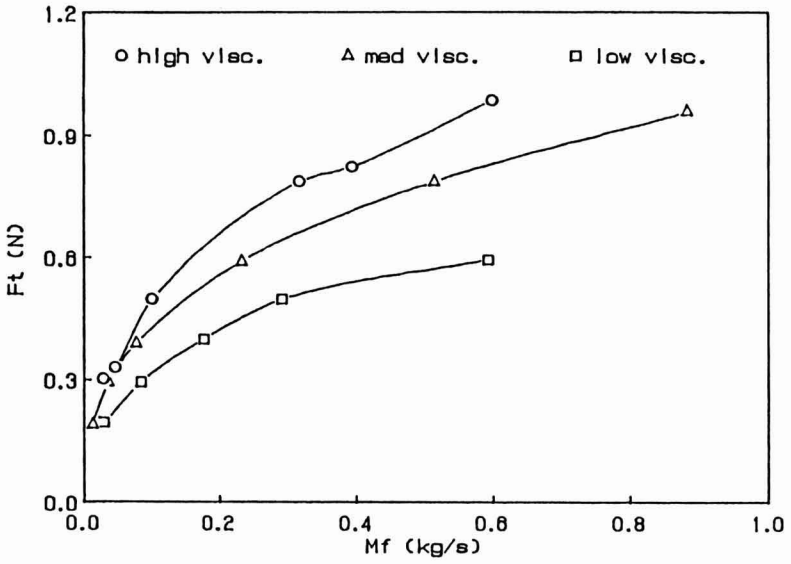
G. SUBRAMANIAM AND C.A. ZURITZ

FIG. 8. TOTAL DRAG FORCE VERSUS MASS FLOW RATE FOR
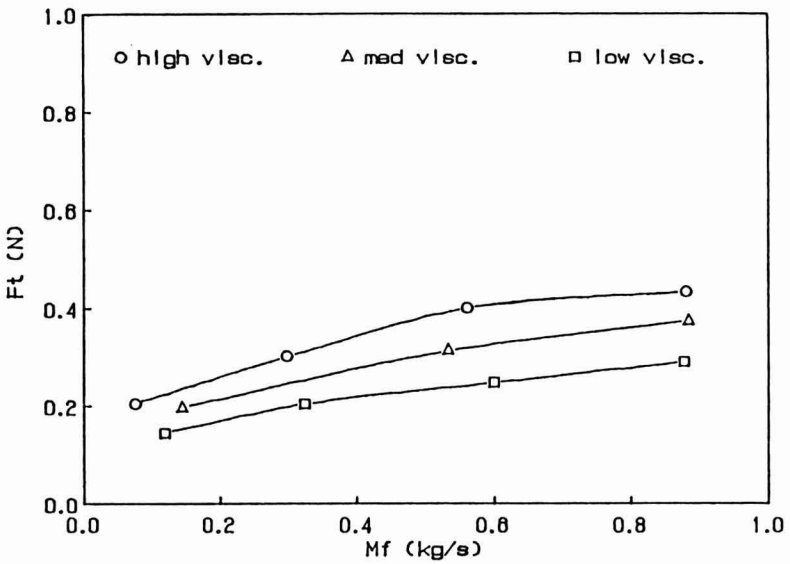THE MEDIUM SPHERE LOCATED AT THE AXIS

FIG. 9. TOTAL DRAG FORCE VERSUS MASS FLOW RATE FOR
THE SMALL SPHERE LOCATED AT THE AXIS

Particles Located Off-Center

When tests were conducted without restrainers, to study the influence of radial location on drag force, it was observed that the large and medium spheres rested against the wall of the tube, whereas the small sphere stayed at a distance (measured from the particle center) of between 0.5 to 1 cm from the tube axis $(0.22 < r/R < 0.41)$. This tended to vary with flow rate. However, an approximate estimate of the location was made for every run.

Off-center drag force versus mass flow rate graphs were also made for the three test spheres. It is seen that the total drag force (F_t) in the case of the small and the medium spheres (Fig. 10 and 11, respectively) does not decrease consistently with decrease in fluid viscosity. In other words, the total drag force measured on the medium sphere at high viscosity was lower than that measured at medium viscosity and in the case of the small sphere, the low viscosity readings exceeded the readings taken at medium viscosity. Only the data obtained with the large sphere (Fig. 12) produced "well-behaved" curves of F_t versus M_f. The above trends were also observed with the net drag force (F_d) on the spheres. These observations could be explained as follows.

(1)   Since the test spheres were of different sizes, their centers were not located at the same radial distance from the tube axis. When the large sphere was touching the wall, its center was much closer to the line of maximum fluid velocity (the tube axis) than that of the medium. Moreover, the small sphere tended to position itself between the tube axis and the wall. Therefore, a comparison of the drag force experienced by particles located at different radial positions, is not entirely justifiable.

(2)   Friction between the particle and the tube wall might have supported some of the pull on the large and medium spheres thus reducing the measured drag.

(3)   In the case of the small sphere, refraction due to the plexiglass tubing made it difficult to exactly measure lengths within the tube (an error of 1 mm in the measurement of the radial position can alter the value of the Reynolds number by up to 2%, which then would be magnified further in the logarithmic scale).

String-and-Sphere Experiments

Similar results were also obtained with the string-and-sphere arrangement. Figure 13 shows the best-fit straight line in a plot of C_{ds}, the drag coefficient of the string, versus $(N_{Re})_t$, the tube Reynolds number (D_{ds} was calculated with an equation similar to Eq. 20). Using this regression ($r^2 = 0.99$), the net drag force on the spheres for corresponding tube Reynolds numbers was obtained as in the case of the wire-and-sphere arrangement.
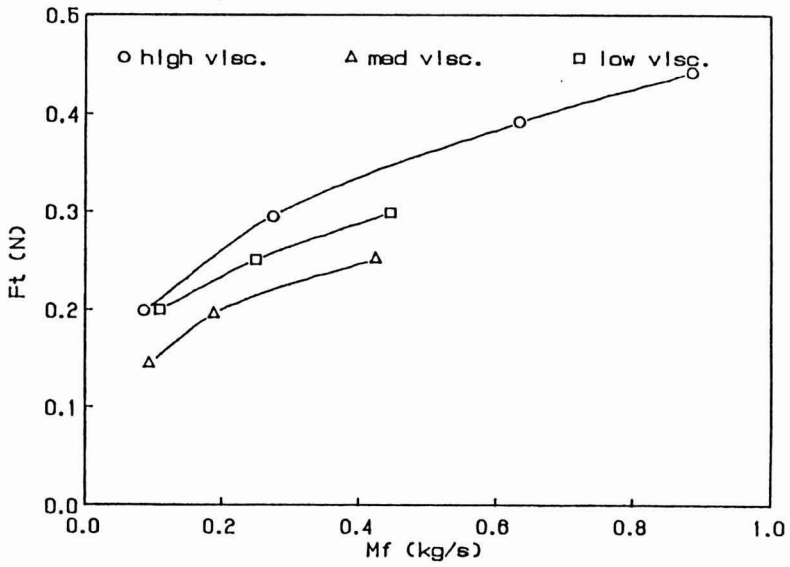
FIG. 10. TOTAL DRAG FORCE VERSUS MASS FLOW RATE FOR
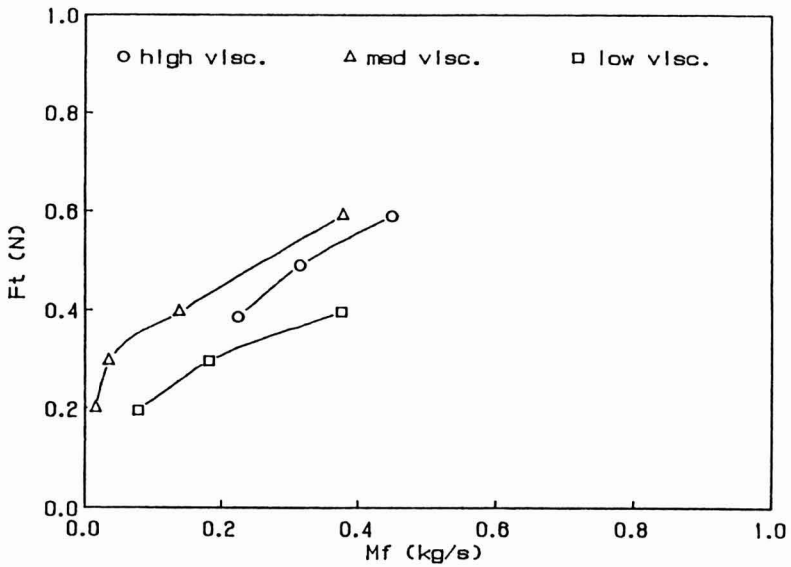THE SMALL SPHERE AT THE WALL

FIG. 11. TOTAL DRAG FORCE VERSUS MASS FLOW RATE FOR
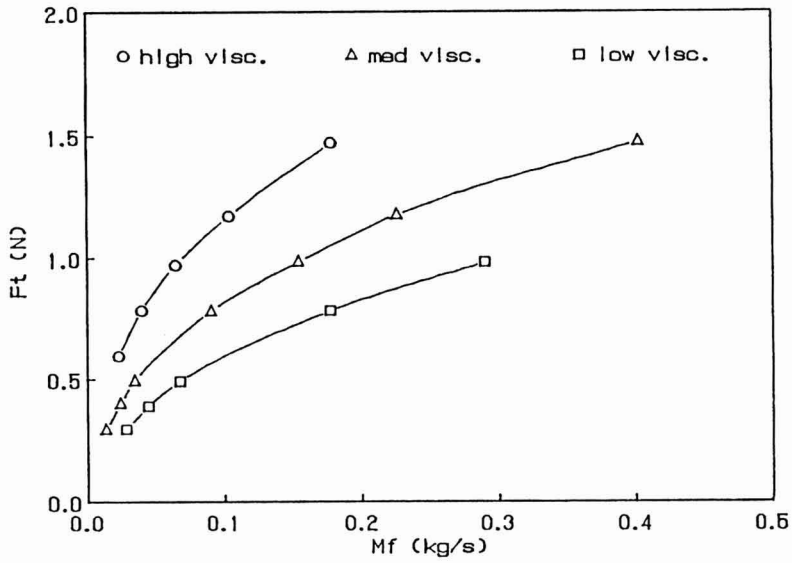THE MEDIUM SPHERE AT THE WALL

FIG. 12. TOTAL DRAG FORCE VERSUS MASS FLOW RATE FOR
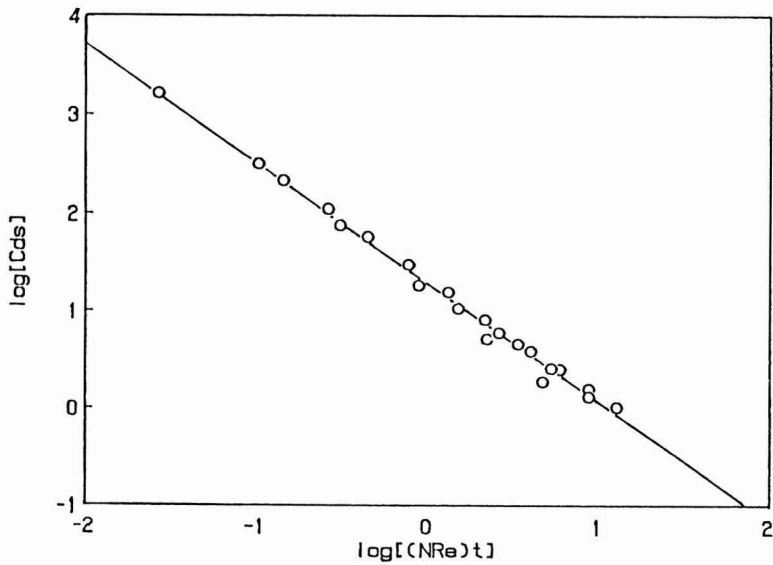THE LARGE SPHERE LOCATED AT THE WALL

FIG. 13. LOGARITHMIC PLOT OF STRING DRAG COEFFICIENT
VERSUS TUBE REYNOLDS NUMBER

The drag coefficient for the particle was obtained using the following defini-
tion (Whitaker 1968).

$$c_d = 2F_d/(\rho A_p v_{f(r)}^2) \tag{21}$$

A log-log plot of the sphere drag coefficient (c_d) versus the Reynolds number-
flow index group, $[(N_{Re})_p]^{1/n}$ for the two data sets combined is shown in Fig.
14. Equation 22 below, represents the combined linear regression line ($r^2 = 0.93$,
$\sigma_y = 0.26$ and $\sigma_s = 0.02$).

$$\log[c_d] = 2.01 - 0.84\log[(N_{Re})_p]^{1/n} \tag{22}$$

or,

$$c_d = 101.35/[(N_{Re})_p]^{0.84/n} \tag{23}$$

The scatter of string data points in Fig. 14 is lesser than for the wire-and-
sphere case. Possible reasons for this phenomenon are listed below.

(1) The string being slightly thicker (0.13 mm) and rougher than the wire
(0.1 mm), offered more resistance to carrier-fluid flow, and thus contributed
relatively more to the total drag force measured. This might have been a stabiliz-
ing factor in the drag force measurements. (A parallel may be drawn in the
behavior of the large sphere, which offered high resistance to flow, and conse-
quently outweighed the experimental errors associated with the drag force
measurements.)

(2) Owing to the higher drag on the string, it was possible to use a greater
number of flow rate settings while testing with the string alone, as compared to
the case of the wire. Consequently, more data points were obtained for the str-
ing, resulting in a better fit for the string drag coefficient.

Considering that the two sets of experiments were conducted independently
using different CMC solutions, one may infer that the above results can be
reproduced in the laboratory with good accuracy. The proposed drag coefficient-
Reynolds number correlation is representative of a single sphere suspended at
any radial location in power law tube flow. In real life situations, particle-
particle and particle-wall interactions will also affect particulate motion.
Therefore, these factors should also be considered while determining residence
time distributions.

A good estimate of the drag force on particles within a holding tube places the
researcher in an advantageous position to determine particle residence times and
predict mechanical damage to the suspended solids. In the food processing in-
dustry, knowledge of the magnitudes of drag forces on suspended food particles
moving through aseptic holding tubes is vital to good system design and process
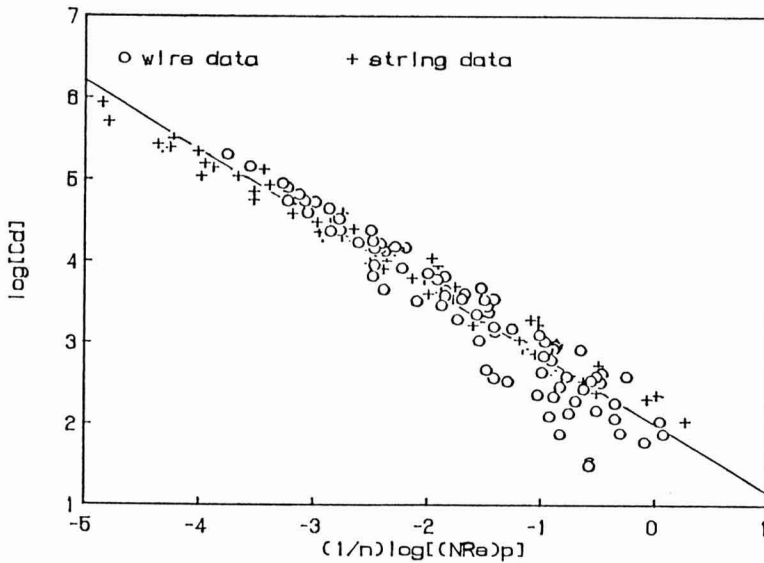
FIG. 14. REGRESSION LINE FOR LOG[[C_d] VERSUS
LOG[$(N_{Re})_p$]$^{1/n}$ FROM WIRE AND STRING DATA SETS

control. Since the present work deals only with spheres, it could be applied to the case of the spherical or nearly spherical food particles such as, peas, potatoes, etc. The suceptibility of food particles to mechanical damage, underscores and importance of the study of drag effects on them during aseptic processing.

CONCLUSIONS

Based on the results of drag measurement and correlation, the following conclusions were drawn.

(1) For a given viscosity and mass flow rate, the largest test sphere experienced the greatest drag force of the three spheres tested.

(2) At given viscosity levels, greater drag force readings were recorded at higher mass flow rates.

(3) For given mass flow rates, the test spheres registered more drag at higher viscosity levels.

(4) In general, the particle drag coefficient was greater at higher generalized particle Reynolds numbers.

(5) The following drag coefficient-Reynolds number correlation: $C_d = 101.35/[(N_{Re})_p]^{0.84/n}$, was developed, and it may be used to estimate drag forces on spherical particles suspended in tube flow of a power law liquid in the generalized particle Reynolds number range $(0.001 - 0.5)$ based on particle-to-fluid relative velocities.

LIST OF SYMBOLS

A	cross sectional area of flow
A_p	projected area of a sphere
C_d	particle drag coefficient
C_{ds}	drag coefficient for the string
C_{dw}	drag coefficient for the wire
D	dimensionless deformation rate tensor
D	inside diameter of the tube
D_c	a characteristic length
D_p	particle (sphere) diameter
$\underline{\nabla}$	gradient vector operator (del) composed of spatial coordinates x_1, x_2, and x_3
$\underline{\nabla}^*$	dimensionless del operator composed of dimensionless spatial coordinates X_1, X_2 and X_3
F_d	net drag force on immersed sphere
F_t	total measured drag force
F_w	drag force on the wire
K_0	dimensionless group representing apparent viscosity
L_e	entrance length
m	fluid consistency index
M_f	mass flow rate of the carrier liquid
n	flow behavior index
N_{BC}	dimensionless group representing boundary conditions
$(N_{Re})_{gen}$	generalized Reynolds number for non-Newtonian (power law) flow
$(N_{Re})_p$	generalized particle Reynolds number
$(N_{Re})_{p,E}$	generalized particle Reynolds number in Ellis fluids
$(N_{Re})_t$	generalized tube Reynolds number for laminar flow
p	thermodynamic system pressure
p	dimensionless pressure
Q	volumetric flow rate of the carrier liquid
r	radial distance from tube axis
r^2	coefficient of determination

R	inside radius of the tube
ϱ	fluid density
σ_y	standard error in Y-estimate
σ_s	standard error in slope
$\underline{U}$	dimensionless velocity vector
$\underline{v}$	velocity vector
v_c	a characteristic velocity
V_{av}	cross-sectional area averaged flow velocity
$V_{f(r)}$	streamline velocity in laminar tube flow, a function of radial position (r)
V_p	particle velocity
V_{pf}	particle-to-fluid relative velocity

REFERENCES

BIZZEL, G.D. and SLATTERY, J.C. 1962. Non-Newtonian boundary layer flow. Chem. Engr. Sci., *17*, 777–782.

CASWELL, B. and SCHWARTZ, W.H. 1962. The creeping motion of a Non-Newtonian fluid past a sphere. J. Fluid Mech. *13*, 417–426.

GOLDSMITH, H.L. and MASON, S.G. 1961. Axial migration of particles in poiseuille flow. Nature, London. *190*(1); 1095–1096.

HAPPEL, J. and BYRNE, B.J. 1954. Motion of a sphere and fluid in a cylindrical tube. J. Industr. Eng. Chem. *46*, 1181–1186.

MHATRE, M.V. and KINTNER, R.C. 1959. Fall of liquid drops through pseudoplastic liquids. Ind. Engr. Chem. *50*(7), 865–867.

ODAR, F. and HAMILTON, W.S. 1963. Forces on a sphere accelerating in a viscous liquid. J. Fluid Mech. *18*, 302–314.

RUBINOW, S.I. and KELLER, J.B. 1961. The transverse force on a spinning sphere moving in a viscous fluid. J. Fluid Mech. *11*, 447–459.

SAFFMAN, P.G. 1965. The lift on a small sphere in a slow shear flow. J. Fluid Mech. *22*(2), 385–400.

SAFFMAN, P.G. 1968. The lift on a small sphere in a slow shear flow. Corrigendum. J. Fluid Mech. *31*, 624.

SASTRY, S.K. and ZURITZ, C.A. 1987. A model for particle suspension flow in a tube. ASAE paper No. 87–6537.

SEGRE, G. and SILBERGERG, A. 1961. Radial particle displacements in poiseuille flow of suspensions. Nature, London, *189*, 209–210.

SKELLAND, A.H.P. *1967.* Non-Newtonian Flow and Heat Transfer. pp. 140–147, John Wiley & Sons, New York.

SLATTERY, J.C. 1960. Flow of a simple Non-Newtonian fluid past a sphere. Appl. Sci. Res. *10*(A), 286–294.

SLATTERY, J.C. and BIRD, R.B. 1961. *Non-Newtonian flow past a sphere. J. Chem. Engng. Sci. 16*, 231–241.

TOMITA, Y. 1959. On the fundamental formula of Non-Newtonian flow. Bull. JSME, 2(7), 469–474.

TRITTON, D.J. 1959. Experiments on the flow past a circular cylinder at low Reynolds numbers. J. Fluid Mech. 6547–567.

WASSERMAN, M.L. and SLATTERY, J.C. 1964. Upper and lower bounds on the drag coefficient of a sphere in a power-model fluid. A.I. ChE. J. *10*, 383–388.

WHITAKER, S. 1968. *Introduction to Fluid Mechanics.* Chapters 4, 5, 7, 8, 11. Prentice-Hall, Englewood Cliffs, N.J.

ZIEGENHAGEN, A.J., BIRD, R.B. and JOHNSON, M.W. 1961. Non-Newtonian flow around a sphere. Trans. Soc. Rheol. 5, 47.

F
N
P
PUBLICATIONS IN
FOOD SCIENCE AND NUTRITION

Journals

JOURNAL OF MUSCLE FOODS, N.G. Marriott and G.J. Flick, Jr.
JOURNAL OF SENSORY STUDIES, M.C. Gacula, Jr.
JOURNAL OF FOOD SERVICE SYSTEMS, O.P. Snyder, Jr.
JOURNAL OF FOOD BIOCHEMISTRY, J.R. Whitaker, N.F. Haard and
   H. Swaisgood
JOURNAL OF FOOD PROCESS ENGINEERING, D.R. Heldman and R.P. Singh
JOURNAL OF FOOD PROCESSING AND PRESERVATION, D.B. Lund
JOURNAL OF FOOD QUALITY, R.L. Shewfelt
JOURNAL OF FOOD SAFETY, T.J. Montville and A.J. Miller
JOURNAL OF TEXTURE STUDIES, M.C. Bourne and P. Sherman

Books

CONTROLLED/MODIFIED ATMOSPHERE/VACUUM PACKAGING OF
   FOODS, A.L. Brody
NUTRITIONAL STATUS ASSESSMENT OF THE INDIVIDUAL, G.E. Livingston
QUALITY ASSURANCE OF FOODS, J.E. Stauffer
THE SCIENCE OF MEAT AND MEAT PRODUCTS, 3RD ED., J.F. Price and
   B.S. Schweigert
HANDBOOK OF FOOD COLORANT PATENTS, F.J. Francis
ROLE OF CHEMISTRY IN THE QUALITY OF PROCESSED FOODS,
   O.R. Fennema, W.H. Chang and C.Y. Lii
NEW DIRECTIONS FOR PRODUCT TESTING AND SENSORY ANALYSIS
   OF FOODS, H.R. Moskowitz
PRODUCT TESTING AND SENSORY EVALUATION OF FOODS,
   H.R. Moskowitz
ENVIRONMENTAL ASPECTS OF CANCER: ROLE OF MACRO AND MICRO
   COMPONENTS OF FOODS, E.L. Wynder et al.
FOOD PRODUCT DEVELOPMENT IN IMPLEMENTING DIETARY
   GUIDELINES, G.E. Livingston, R.J. Moshy, and C.M. Chang
SHELF-LIFE DATING OF FOODS, T.P. Labuza
RECENT ADVANCES IN OBESITY RESEARCH, VOL. V, E. Berry,
   S.H. Blondheim, H.E. Eliahou and E. Shafrir
RECENT ADVANCES IN OBESITY RESEARCH, VOL. IV, J. Hirsch et al.
RECENT ADVANCES IN OBESITY RESEARCH, VOL. III, P. Bjorntorp et al.
RECENT ADVANCES IN OBESITY RESEARCH, VOL. II, G.A. Bray
RECENT ADVANCES IN OBESITY RESEARCH, VOL. I, A.N. Howard
ANTINUTRIENTS AND NATURAL TOXICANTS IN FOOD, R.L. Ory
UTILIZATION OF PROTEIN RESOURCES, D.W. Stanley et al.
FOOD INDUSTRY ENERGY ALTERNATIVES, R.P. Ouellette et al.
VITAMIN B_6: METABOLISM AND ROLE IN GROWTH, G.P. Tryfiates
HUMAN NUTRITION, 3RD ED., F.R. Mottram
FOOD POISONING AND FOOD HYGIENE, 4TH ED., B.C. Hobbs et al.
POSTHARVEST BIOLOGY AND BIOTECHNOLOGY, H.O. Hultin and M. Milner

Newsletters

FOOD INDUSTRY REPORT, G.C. Melson
FOOD, NUTRITION AND HEALTH, P.A. Lachance and M.C. Fisher
FOOD PACKAGING AND LABELING, S. Sacharow

GUIDE FOR AUTHORS

Typewritten manuscripts in triplicate should be submitted to the editorial office. The typing should be double-spaced throughout with one-inch margins on all sides.

Page one should contain: the title, which should be concise and informative; the complete name(s) of the author(s); affiliation of the author(s); a running title of 40 characters or less; and the name and mail address to whom correspondence should be sent.

Page two should contain an abstract of not more than 150 words. This abstract should be intelligible by itself.

The main text should begin on page three and will ordinarily have the following arrangement:

Introduction: This should be brief and state the reason for the work in relation to the field. It should indicate what new contribution is made by the work described.

Materials and Methods: Enough information should be provided to allow other investigators to repeat the work. Avoid repeating the details of procedures which have already been published elsewhere.

Results: The results should be presented as concisely as possible. Do not use tables *and* figures for presentation of the same data.

Discussion: The discussion section should be used for the interpretation of results. The results should not be repeated.

In some cases it might be desirable to combine results and discussion sections.

References: References should be given in the text by the surname of the authors and the year. *Et al.* should be used in the text when there are more than two authors. All authors should be given in the Reference section. In the Reference section the references should be listed alphabetically. See below for style to be used.

DEWALD, B., DULANEY, J.T., and TOUSTER, O. 1974. Solubilization and polyacrylamide gel electrophoresis of membrane enzymes with detergents. In *Methods in Enzymology,* Vol. xxxii, (S. Fleischer and L. Packer, eds.) pp. 82–91, Academic Press, New York.

HASSON, E.P. and LATIES, G.G. 1976. Separation and characterization of potato lipid acylhydrolases. Plant Physiol. *57,*142–147.

ZABORSKY, O. 1973. *Immobilized Enzymes,* pp. 28–46, CRC Press, Cleveland, Ohio.

Journal abbreviations should follow those used in *Chemical Abstracts.* Responsibility for the accuracy of citations rests entirely with the author(s). References to papers in press should indicate the name of the journal and should only be used for papers that have been accepted for publication. Submitted papers should be referred to by such terms as "unpublished observations" or "private communication." However, these last should be used only when absolutely necessary.

Tables should be numbered consecutively with Arabic numerals. The title of the table should appear as below:

Table 1. Activity of potato acyl-hydrolases on neutral lipids, galactolipids, and phospholipids

Description of experimental work or explanation of symbols should go below the table proper. Type tables neatly and correctly as tables are considered art and are not typeset. Single-space tables.

Figures should be listed in order in the text using Arabic numbers. Figure legends should be typed on a separate page. Figures and tables should be intelligible without reference to the text. Authors should indicate where the tables and figures should be placed in the text. Photographs must be supplied as glossy black and white prints. Line diagrams should be drawn with black waterproof ink on white paper or board. The lettering should be of such a size that it is easily legible after reduction. Each diagram and photograph should be clearly labeled on the reverse side with the name(s) of author(s), and title of paper. When not obvious, each photograph and diagram should be labeled on the back to show the top of the photograph or diagram.

Acknowledgments: Acknowledgments should be listed on a separate page.

Short notes will be published where the information is deemed sufficiently important to warrant rapid publication. The format for short papers may be similar to that for regular papers but more concisely written. Short notes may be of a less general nature and written principally for specialists in the particular area with which the manuscript is dealing. Manuscripts which do not meet the requirement of importance and necessity for rapid publication will, after notification of the author(s), be treated as regular papers. Regular papers may be very short.

Standard nomenclature as used in the engineering literature should be followed. Avoid laboratory jargon. If abbreviations or trade names are used, define the material or compound the first time that it is mentioned.

EDITORIAL OFFICES: DR. D.R. HELDMAN, COEDITOR, *Journal of Food Process Engineering,* National Food Processors Association, 1401 New York Avenue, N.W., Washington, D.C. 20005 USA; or DR. R.P. SINGH, COEDITOR, *Journal of Food Process Engineering,* University of California, Davis, Department of Agricultural Engineering, Davis, CA 95616 USA.

CONTENTS